200
11-21-80
7+C

2

Dr. 2036

ORNL/TM-6991

ornl

OAK
RIDGE
NATIONAL
LABORATORY

UNION
CARBIDE

Simulated Fission Product—SiC Interaction in Triso-Coated LEU or MEU HTGR Fuel Particles

R. L. Pearson
T. B. Lindemer
E. C. Beahm

MASTER

OPERATED BY
UNION CARBIDE CORPORATION
FOR THE UNITED STATES
DEPARTMENT OF ENERGY

ORNL/TM-6991
Dist. Category UC-77

Contract No. W-7405-eng-26

CHEMICAL TECHNOLOGY DIVISION

HTGR BASE TECHNOLOGY PROGRAM
HTGR Chemistry Studies
(Activity No. AG 25 05; FTP/A 01329)

SIMULATED FISSION PRODUCT—SiC INTERACTION IN TRISO-COATED LEU OR MEU HTGR FUEL PARTICLES

R. L. Pearson
T. B. Lindemer
E. C. Beahm

Date Published: November 1980

OAK RIDGE NATIONAL LABORATORY
Oak Ridge, Tennessee 37830
operated by
UNION CARBIDE CORPORATION
for the
DEPARTMENT OF ENERGY

CONTENTS

SIMULATED FISSION PRODUCT—SiC INTERACTION IN TRISO-COATED LEU OR MEU HTGR FUEL PARTICLES

R. L. Pearson
T. B. Lindemer
E. C. Beahm

ABSTRACT

Proliferation issues relating to the use of highly enriched uranium (HEU) have led to an evaluation of the fission product—SiC interaction problems that might arise if low enriched uranium (LEU) or medium enriched uranium (MEU) were used as fissile fuel in HTGR systems. Simulated Triso-coated UO_2, UC_2, and UO_2/UC_2 particles mixed with varying amounts of Mo, Ru, Rh, Pd, Ag, and Cd were prepared. These fission products were chosen because, after full burnup, their concentrations are higher in LEU and MEU fuels than in HEU fuel. After the particles were heat treated in the laboratory, their behavior was examined by use of metallography, scanning electron microscopy, and electron microprobe x-ray analysis. Ruthenium, rhodium, palladium, and silver were shown to interact with the SiC layer. The palladium-SiC interaction was the most severe. The rate of SiC thinning as a function of temperature was determined for rhodium and palladium. Kernel composition did not seem to influence the SiC thinning rate due to the Pd-SiC interaction. Palladium in UO_2 kernels, after it reached the SiC layer, probably formed silicides and a low-melting, palladium-rich eutectic. Palladium in UC_2 and UO_2/UC_2 kernels probably formed UPd_3 or a U-Pd-Si-C compound throughout the iLTI and SiC layers.

---

1. INTRODUCTION

Prior to 1977, the reference fuel cycle for the high-temperature gas-cooled reactor (HTGR) was the highly enriched uranium (HEU)* cycle. Concerns about nuclear proliferation with the HEU cycle led to an evaluation of the performance of low enriched uranium (LEU)† and medium enriched uranium (MEU)‡ fissile fuels.

---

*HEU — defined as fuel with 93% ^{235}U.
†LEU — defined as fuel with less than 10% ^{235}U.
‡MEU — defined as fuel with less than 20% ^{235}U.

One of the possible performance limitations that has been identified in past irradiation experiments with Triso-coated HTGR fuel particles is chemical interaction between the SiC layer and several of the fission products. In irradiated HEU UC_2 fuel particles, the main interacting fission products are the rare earths,[1-4] whereas in irradiated LEU fuel particles, palladium is the main interacting fission product.[5-9] Palladium is also the main interacting fission product in irradiated PuO_{2-x} and $Th_{0.75}Pu_{0.25}O_{2-x}$ fuel particles.[9] Laboratory experiments using several simulated fission products have resulted in two papers[10,11] that attempt to explain, in detail, fission product behavior in various Triso-coated HEU HTGR fuels. In LEU or MEU fuel, both uranium and plutonium fission results in a different fission product spectrum. At design burnup, several of the fission products have higher concentrations in LEU or MEU fuel than they have in HEU fuel. This report describes which fission products will have greater concentrations, the preparation of Triso-coated particles containing simulated fission products with either UO_2, UC_2, or UO_2/UC_2 kernels, and the investigation of the interaction of the kernels with SiC during heat treatment.

2. EXPERIMENTAL PROCEDURE

2.1 Selection of Kernel Compositions

Several of the fission product interactions with SiC which need to be investigated in LEU or MEU fuels may be different from those which have already been investigated in HEU fuels. This is because the ratio of the fissioning isotopes (^{235}U, ^{239}Pu, ^{241}Pu) differs as the uranium enrichment changes and because the fission yield from each isotope is not the same. An analysis of the fission product inventories in various HTGR fuels is found in Appendix A; after full burnup, those fission products that have greater inventories in typical LEU or MEU fuel particles are Mo, Ru, Rh, Pd, Ag, and Cd (Appendix A, Table A.2).

Two sets of Triso-coated kernels were prepared for this study. The first set was used for an exploratory investigation, while the second set was refined to provide more specific results. The first set of kernel compositions is listed in Table 1. (Compositions of all samples listed in Table 1 are calculated in Appendix B.) Sample 1-1 was an attempt to duplicate the metallic inclusions found within a Triso-coated MEU UO_2 particle irradiated to 20% FIMA.[12] The inclusions are a homogeneous alloy of the noble metals Ru, Tc, Rh, Pd, and some Mo. Technetium was not included in the simulated mixture because it exists only as a radioactive isotope. Sample 1-2 is the same fission product mixture added to a UC_2 kernel. Uranium carbide forms compounds with these fission products, which may influence the fission product interaction with SiC. These fission product compounds with uranium will be discussed in more detail in Sect. 4. Sample 1-3 is a UO_2-Ag mixture. One hundred times more silver was added than will be present in an MEU UO_2 particle irradiated to 20% FIMA. The purpose of the extra silver was twofold: First, one may need to compensate for silver loss because of its high vapor pressure at coating temperatures (Fig. 1). Second, the normal amount of silver in an MEU UO_2 fuel irradiated to full burnup is barely enough to detect with our x-ray equipment.

Our second set of samples was prepared after some experience with the first set. In the first set, identification of rhodium and palladium individually was impossible because of their nearly identical x-ray characteristics in the electron microprobe (EMP). In samples 2-1 and 2-2, rhodium and palladium were separated so that we could positively identify the behavior of each. Lanthanum was added to sample 2-3 to determine if there is a synergistic effect when a mixture of ruthenium, palladium, and lanthanum reacts with the SiC layer. In samples 2-4 and 2-5, the metallic inclusion alloy was dispersed in UO_2 to more closely simulate an irradiated UO_2 particle than did sample 1-1. Samples 2-6 and 2-7 were prepared to investigate the effect a UO_2/UC_2 fuel mixture would have on the fission product interaction with SiC. Sample 2-8 is another UO_2-Ag mixture, but the silver concentration more closely simulates the silver concentration in MEU UO_2 at full burnup. Finally, sample 2-9 is an attempt to include cadmium in a UO_2 fuel particle.

Table 1. Triso-coated particles prepared for evaluation

Sample	Batch	Kernel composition (wt %)
		Set 1
1-1	OR-2772	52.1 Mo, 28.5 Ru, 9.0 Rh, 10.4 Pd
1-2	OR-2773	12.5 Mo, 6.0 Ru, 1.4 Rh, 0.9 Pd, 77.0 UC_2, 1.9 C
1-3	OR-2775	3.3 Ag, 96.7 UO_2
		Set 2
2-1	OR-2809	8.2 Mo, 6.9 Ru, 3.0 Pd, 80.2 UC_2, 1.8 C
2-2	OR-2812	8.4 Mo, 5.4 Ru, 1.8 Rh, 82.5 UC_2, 1.9 C
2-3	OR-2814	7.7 Mo, 6.5 Ru, 2.8 Pd, 5.5 La, 75.8 UC_2, 1.7 C
2-4	OR-2822	8.1 Mo, 6.8 Ru, 2.9 Pd, 82.2 UO_2
2-5	OR-2806	8.3 Mo, 5.3 Ru, 1.8 Rh, 84.6 UO_2
2-6	OR-2823	5.4 Mo, 4.6 Ru, 2.0 Pd, 79.5 UO_2, 8.5 UC_2
2-7	OR-2807	5.5 Mo, 4.6 Ru, 2.0 Pd, 57.9 UO_2, 30.0 UC_2
2-8	OR-2815	0.4 Ag, 99.6 UO_2
2-9	OR-2808	3.7 CdO, 6.8 SrO, 89.5 UO_2
2-10	GA-VSM 6151-00-035	100 UC_2

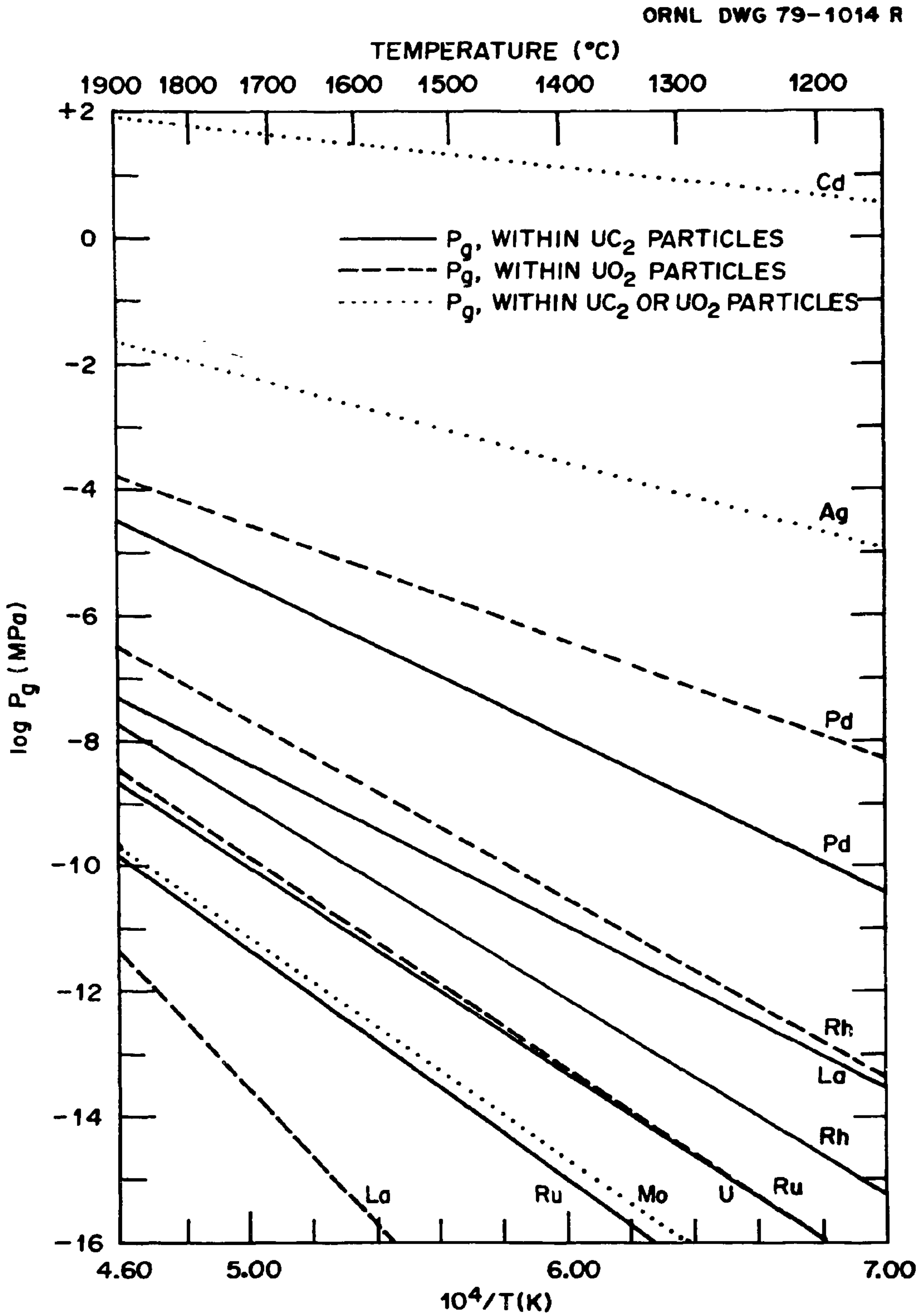

Fig. 1. Vapor pressure of pertinent simulated fission product—fuel mixes versus reciprocal temperature (calculated using SOLGASMIX-PV[20]).

2.2 Kernel Preparation and Characterization

The kernels were made and then Triso coated.[13] Each compound or element was obtained as a powder and sieved through a 325-mesh screen. The powder mixture was blended intimately in a Spex* shaker as an ethyl alcohol slurry, which was then dried in a vacuum. All of the mixtures that contained UO_2 were hot pressed into pellets. The UO_2 plus fission product samples were made into buttons in an arc-melting furnace in an argon atmosphere. The desired kernel sizes were obtained by crushing and sieving the buttons or pellets. Dimensions of the coated particles are given in Table 2.

Each of the samples listed in Table 1 was mounted, polished, and analyzed by energy-dispersive x rays generated by an EMP or scanning electron microprobe (SEM) to ensure that all of the simulated fission products could be identified qualitatively. The detection limit of the elements with use of the dispersive x-ray unit is approximately 0.1%. All of the fission products except those in batches OR-2814, OR-2815, and OR-2808 were easily identified, as described more fully below. Those kernels containing UO_2 were coated with the inner low-temperature isotropic (iLTI) layer in a gas mixture containing 10 vol % CO, which was added to maintain O/U = 2.000 via the C-CO-O_2 equilibrium. The purpose of this treatment was to coat kernels having an oxygen chemical potential[14] approximately the same as that in irradiated oxide fuel particles.

Coating the silver- and cadmium-containing kernels introduced a special set of problems. Silver, cadmium, and their compounds have very high vapor pressures (Fig. 1) at 1473 to 1573 K, the optimum temperature range used to form the buffer and iLTI layers.[13] The silver-containing particles in the first set of samples were successfully prepared by first depositing a thick, gas-tight pyrolytic carbon sealer layer around the kernel. This layer was deposited at 1073 K, then at 1173 K to avoid a high silver vapor pressure during the deposition. The remaining layers were then formed at optimum conditions.

---

*Spex Industries, Inc., P.O. Box 798, Metucken, N.J. 08840.

Table 2. Dimensions of Triso-coated particles prepared for this study

Sample	Batch	Kernel diameter (μm)	Buffer thickness (μm)	Inner LTI thickness (μm)	SiC thickness (μm)	Outer LTI thickness (μm)
1-1	OR-2772	300-420	69	34	79	69
1-2	OR-2773	300-420	132	43	58	78
1-3	OR-2775	354-420	153[a]	63	52	81
2-1	OR-2809	300-420	63	41	43	45
2-2	OR-2812	300-420	48	41	40	42
2-3	OR-2814	300-420	66	38	42	43
2-4	OR-2822	300-420	69	46	39	45
2-5	OR-2806	300-420	85	53	40	54
2-6	OR-2823	300-420	73	55	40	44
2-7	OR-2807	300-420	99	56	49	43
2-8	OR-2815	300-420	63[b]	48	40	27
2-9	OR-2808	300-420	58[b]	48	39	47
2-10	GA-VSM 6151-00-035	196	99	33	32	38

[a]Includes 53-μm sealer layer next to kernel.

[b]Includes ∼5-μm sealer layer next to kernel.

An unsuccessful attempt to form cadmium-containing particles was made in batch OR-2808 by mixing SrO with CdO to form a solid solution. Apparently this did not lower the vapor pressure of cadmium enough, since it was lost during coating of the kernels. Also, the sealer layers formed around the kernels in samples 2-8 and 2-9 were not as thick as the sealer layer in sample 1-3. Apparently the silver and cadmium were able to escape as the iLTI layer was applied. The iLTI layer of sample 2-9 was porous, as discussed below.

The lanthanum in batch OR-2814 could barely be identified. The cause for the loss of lanthanum cannot be fully explained, but it may have been due to a defective iLTI layer.

2.3 Characterization of iLTI Layer

Hot chlorine leach tests,[15] which were performed on a few particles from each batch before application of the SiC layer, indicated that all but three of the as-made batches listed in Table 1 had impermeable iLTI layers. This conclusion was drawn because no change was observed in radiographs taken before and after a 3-h chlorine treatment at 1773 K. The three batches with part of the kernels leached away were OR-2772, with 19% of the kernels removed; OR-2809, with 4% removed; and OR-2808, with 10% removed. No chlorine could be detected in SEM x-ray patterns of any of the completed Triso-coated particles, even the three batches whose iLTI layers were identified as porous.

The densities of the iLTI layers of several batches were suspect. After heating isothermally at 1673 K for 820 h, wafers filled with particles from batches OR-2809, OR-2812, and OR-2814 were mounted and polished to midplane. The iLTI layers appeared full of holes, particularly at the SiC interface. Sometimes the iLTI layer pulled away from the SiC and formed a gap.

2.4 Characterization of SiC Layer

The condition of the as-deposited SiC coatings of the samples listed in Table 1 was assessed. Several particles from each batch were mounted, polished, and etched in a boiling 1:1 mixture of saturated solutions of $K_2Fe(CN)_6$ and NaOH to expose the microstructure of the SiC layer. Typical microstructures can be seen in Fig. 2. The results were compared to the microstructures found in a previous SiC coating study,[16] and the conclusions drawn are listed in Table 3. The only SiC coating with serious flaws was found in batch OR-2772. No elements other than silicon could be detected by dispersive x-ray analysis within any of the SiC layers. (Carbon is not detectable with these units.)

2.5 Heat Treatment

About 20 particles from each batch were enclosed at the midplane of a 12.5-mm-diam carbon disk and heated in a graphite-resistance furnace where a known temperature and a temperature gradient of 27.8 K/mm were maintained. As an example, a wafer heated at a maximum of 2175 K would contain particles with temperatures of 1825 to 2175 K. The details of the procedure used to prepare particles for heat treatment have been published previously.[17]

2.6 Examination of Particles

The fission product interaction with SiC was followed by several methods. The extent of interaction during heat treatment was estimated by periodically turning off the furnace and radiographing the wafer. After the heat treatment was completed, the samples were mounted and polished to midplane. The condition of the polished SiC surface was observed with an optical microscope under bright-field illumination and sometimes with an SEM. The condition of the SiC layer under the polished surface could be evaluated because the SiC was translucent and could be examined in a stereomicroscope under either polarized or oblique light. Both the identity and the movement of the heavy metals within the particles, including the SiC layer, were determined by using the x-ray capabilities of either the SEM or the EMP.

ORNL-PHOTO Y167278

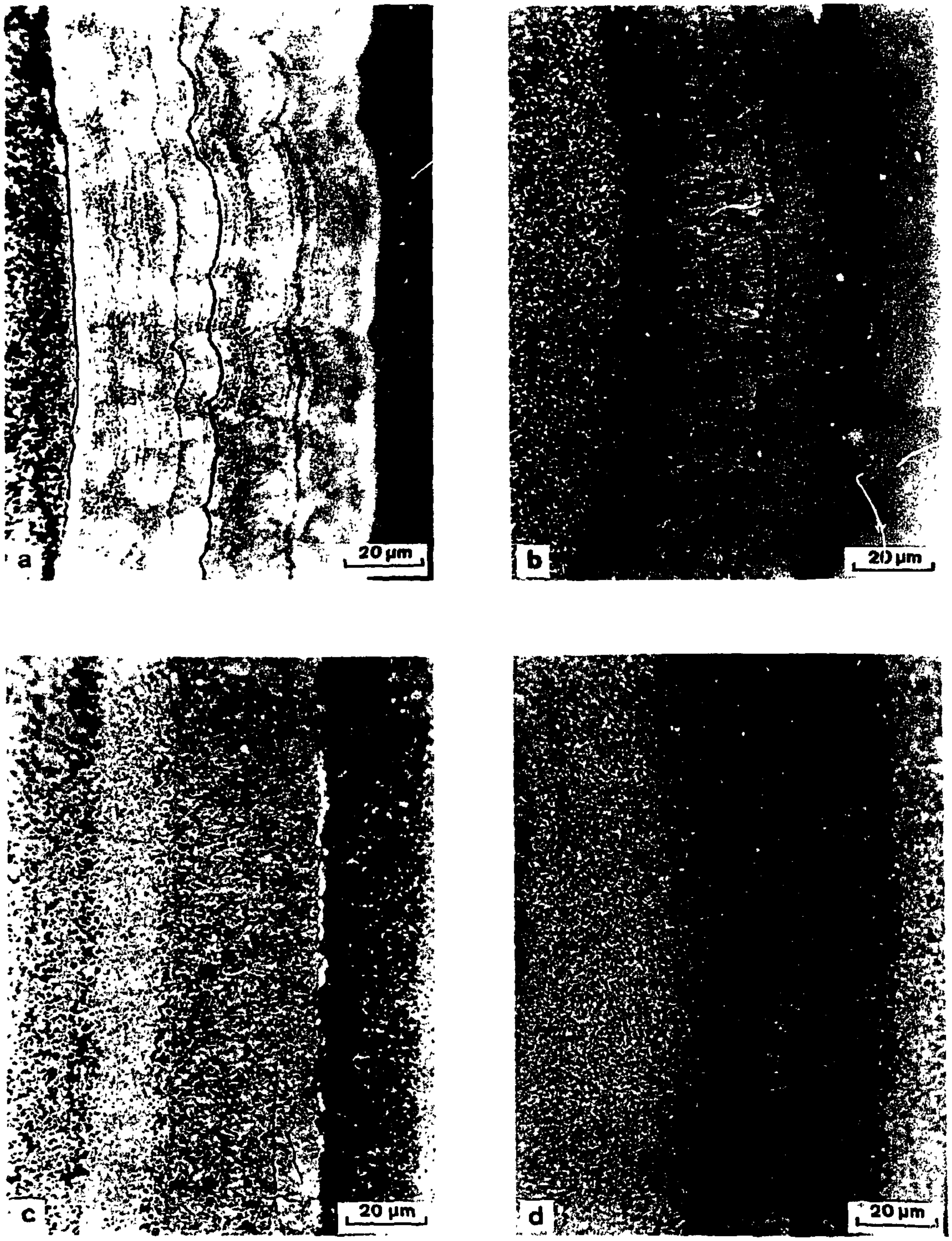

Fig. 2. Optical micrographs showing microstructural detail of the as-made SiC layers. (*a*) Triso-coated Mo-Ru-Rh-Pd alloy particle (batch OR-2772); (*b*) Triso-coated UO_2 plus Ag (OR-2775); (*c*) Triso-coated UC_2 plus Mo-Ru-Pd particle (OR-2809); (*d*) Triso-coated 90% UO_2/10% UC_2 plus Mo-Ru-Pd particle (OR-2823).

Table 3. Analysis of as-deposited SiC coatings used in fission product–SiC interface study

Sample	Batch	Estimated SiC deposition temperature (K)	Comments
1-1	OR-2772	1750	Questionable coating; circumferential porosity.
1-2	OR-2773	1750	Possibly some porosity.
1-3	OR-2775	1850	Good coating.
2-1	OR-2809	1820	Numerous circumferential cracks; scattered porosity; some large voids.
2-2	OR-2812	1820	Circumferential cracks; some porosity; very disordered appearance for inner half thickness.
2-3	OR-2814	1820	Circumferential bands of porosity and a few cracks; grain structure seemingly acceptable, but difficult to observe due to light etch.
2-4	OR-2822	1820	Fairly good structure.
2-5	OR-2806	1820	Numerous bands of porosity; appeared to be a large crack close to the iLTI layer.
2-6	OR-2823	1820	Good grain structure; very little porosity; no obvious cracks.
2-7	OR-2807	1820	Numerous bands of porosity and interrupted growth; one or two cracks present.
2-8	OR-2815	1820	Some bands of porosity; a few cracks close to the surface; otherwise, fairly good grain structure.
2-9	OR-2808	1820	Numerous cracks; several bands of porosity; appeared to be some radial cracks originating at outside surface.
2-10	GA-VSM 6151-00-035	1820	Fairly good coating; no obvious cracks or porosity; deposition conditions unknown.

3. RESULTS FROM HEAT-TREATED PARTICLES

Wafers containing particles prepared for this study (Table 2) were heat treated as described in Table 4. The results of these heat treatments are reported in this section.

Table 4. Heat treatment schedules of fission product—SiC interaction studies

Kernel composition	Sample (batch)	Wafer No.	Maximum heat treatment temperature[a] (K)	Time (h)
Mo-Ru-Rh-Pd	1-1 (OR-2772)	1	2173	25
		2	2023	24
		3	1773	3528
UO_2 + (SrO-CdO)	2-9 (OR-2808)	1	2173	215
UO_2 + (Mo-Ru-Pd)	2-4 (OR-2822)	1	2173	215
UO_2 + (Mo-Ru-Rh)	2-5 (OR-2806)	1	2173	215
UO_2 + Ag	1-3 (OR-2775)	1	2173	25
		2	2023	260
		3	1773	3528
UC_2	2-10 (GA-VSM)	1	2173	215
UC_2 + (Mo-Ru-Rh-Pd)	1-2 (OR-2773)	1	2173	50
		2	2023	260
		3	1773	3528
UC_2 + (Mo-Ru-Pd)	2-1 (OR-2809)	1	2173	25
		2	2173	90
		3	1873	50
UC_2 + (Mo-Ru-Rh)	2-2 (OR-2812)	1	2173	25
		2	2173	90
		3	1873	100
UC_2 + (Mo-Ru-Pd-La)	2-3 (OR-2814)	1	2173	50
		2	2173	90
		3	1873	50
65% UO_2/35% UC_2 + (Mo-Ru-Pd)	2-7 (OR-2807)	1	2173	215
90% UO_2/10% UC_2 + (Mo-Ru-Pd)	2-6 (OR-2823)	1	2173	215

[a]All heat treatments conducted with a thermal gradient of 27.8 K/mm.

3.1 Triso-Coated Particles Containing Mo-Ru-Rh-Pd

Twenty particles of sample 1-1 (batch OR-2772) were embedded in three separate wafers. Each was heat treated in a temperature gradient of 27.8 K/mm - one at 2173 K for 25 h, another at 2023 K for 24 h, and the third at 1773 K for 3528 h. The kernel alloy that contained only metallic Mo, Ru, Rh, and Pd was extremely corrosive. All of the SiC layers in the particles heated at 2173 K and 2023 K were breached, usually on the hot side of the particles,* and many of the SiC layers in the particles heated at 1773 K were also breached. An example of a particle that was heated at 1490 K for 3582 h is shown in Fig. 3. The material deposited along the circumferential lines in the SiC layer was identified by dispersive x-ray analysis using an EMP to be mainly ruthenium and rhodium. Some palladium and rhodium remained within the inner carbon layers, and some ruthenium and rhodium reached the outer LTI (oLTI) layer. Most of the palladium, which has the highest vapor pressure, escaped. Except for molybdenum, all of these fission products are apparently quite mobile.

3.2 Triso-Coated Particles Containing UO_2

3.2.1 UO_2 only

No Triso-coated particles containing only UO_2 were available to verify that pure UO_2 kernels will not interact with the SiC layer. Instead, 20 particles of sample 2-9 (batch OR-2808), whose cadmium had escaped, were embedded in a graphite matrix and heat treated at 2173 K for 215 h in a temperature gradient of 27.8 K/mm. No interaction in any of the SiC layers could be detected. It was concluded that since UO_2-SrO kernels did not interact, UO_2 kernels will almost certainly not interact either.

---

*Note: In a 27.8 K/mm temperature gradient, a particle with a 500-μm diam will be 14 K hotter on one side than it will be on the other, whereas a 600-μm-diam particle will be 17 K hotter on one side than on the other.

ORNL-PHOTO Y167290

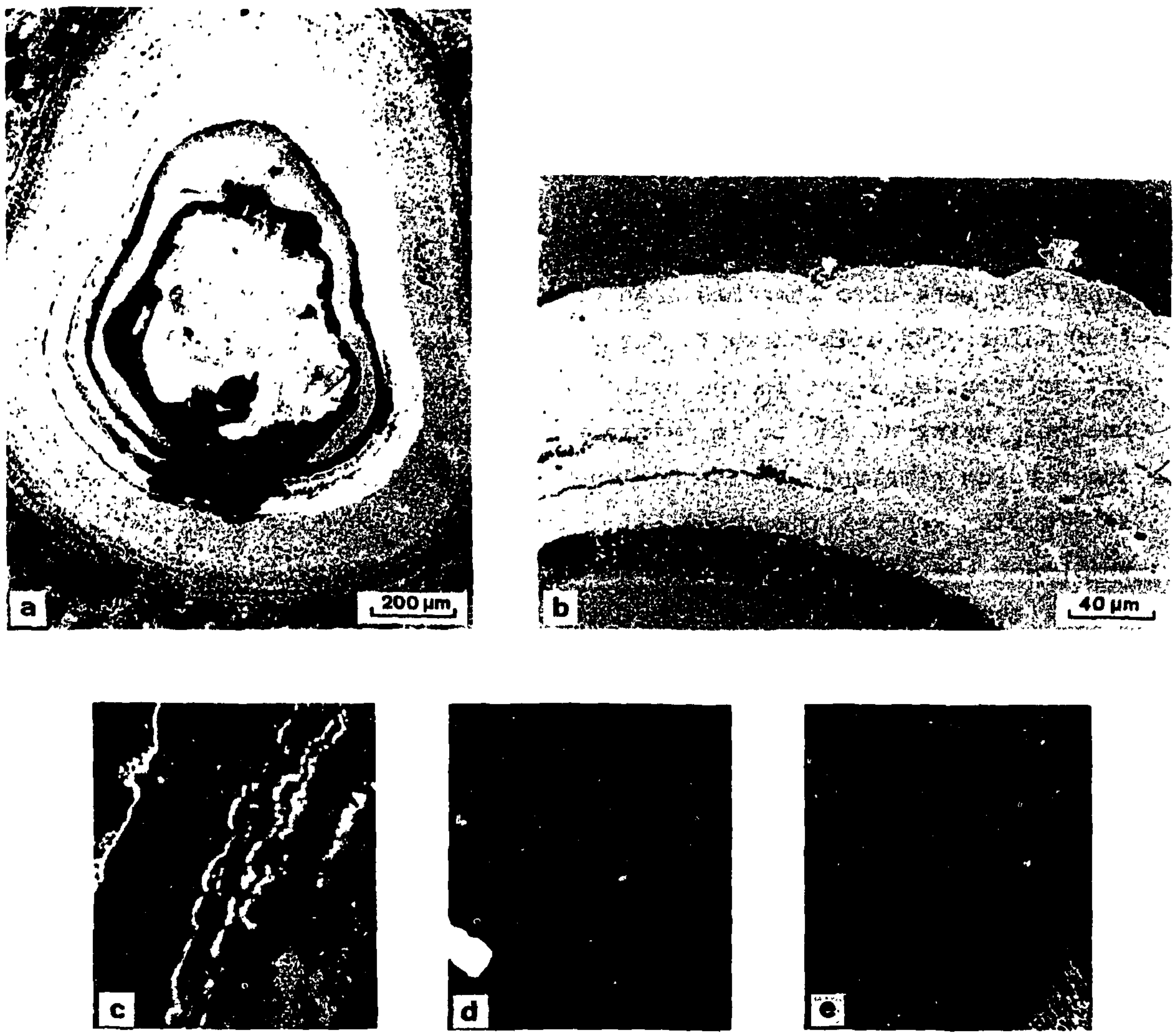

Fig. 3. Triso-coated Mo-Ru-Rh-Pd alloy particle (batch OR-2772) polished to midplane after being heated at 1490 K for 3528 h in a 27.8 K/mm temperature gradient. (*a*) Optical micrograph; (*b*) optical micrograph; (*c*) backscattered electron image of SiC layer; (*d*) Ru L_{α} x rays; (*e*) Rh L_{β} x rays.

3.2.2 UO_2 plus Mo-Ru-Pd

Twenty particles of sample 2-4 (batch OR-2822) were embedded in a graphite matrix and heat treated at 2173 K for 215 h in a temperature gradient of 27.8 K/mm. Interaction between the kernel and the SiC layer occurred in most of the particles. In an optical microscope under bright-field illumination, a second, white phase was seen in the polished SiC surface. One such particle, held at 2063 K, is shown in Fig. 4. The attack points appeared to be randomly distributed between the hot and cold sides of the particle. In a stereomicroscope using polarized light, these white phases were seen to extend into the SiC. They are more accurately described as irregularly shaped nodules within the translucent SiC layer. The white phases seen on the surface were only portions of the nodules that had been exposed by polishing. Palladium and ruthenium were identified by energy-dispersive x rays to be within the nodules. Palladium and ruthenium - but not uranium - were found in the white phases lying within the iLTI and/or at the iLTI-SiC interface.

3.2.3 UO_2 plus Mo-Ru-Rh

Twenty particles of sample 2-5 (batch OR-2806) were embedded in a graphite matrix and heat treated at 2173 K for 215 h in a temperature gradient of 27.8 K/mm. Some SiC interaction occurred randomly in a few of the particles. An example of such a reaction can be seen in Fig. 5; the particle was heated at 2008 K. Energy-dispersive x-ray analysis identified only rhodium in the nodules within the SiC. The white phase within the iLTI layer and/or at the iLTI-SiC interface contained both ruthenium and rhodium.

3.2.4 UO_2 plus Ag

Twenty particles of sample 1-3 (batch OR-2775) were embedded in three separate graphite wafers. Each was heat treated in a temperature gradient of 27.8 K/mm - one at 2173 K for 25 h, another at 2023 K for 260 h, and the third at 1773 K for 3528 h. In many of the particles, as seen in Fig. 6, silver interacted with the SiC layers at several points. Also, silver was

ORNL-PHOTO Y167283

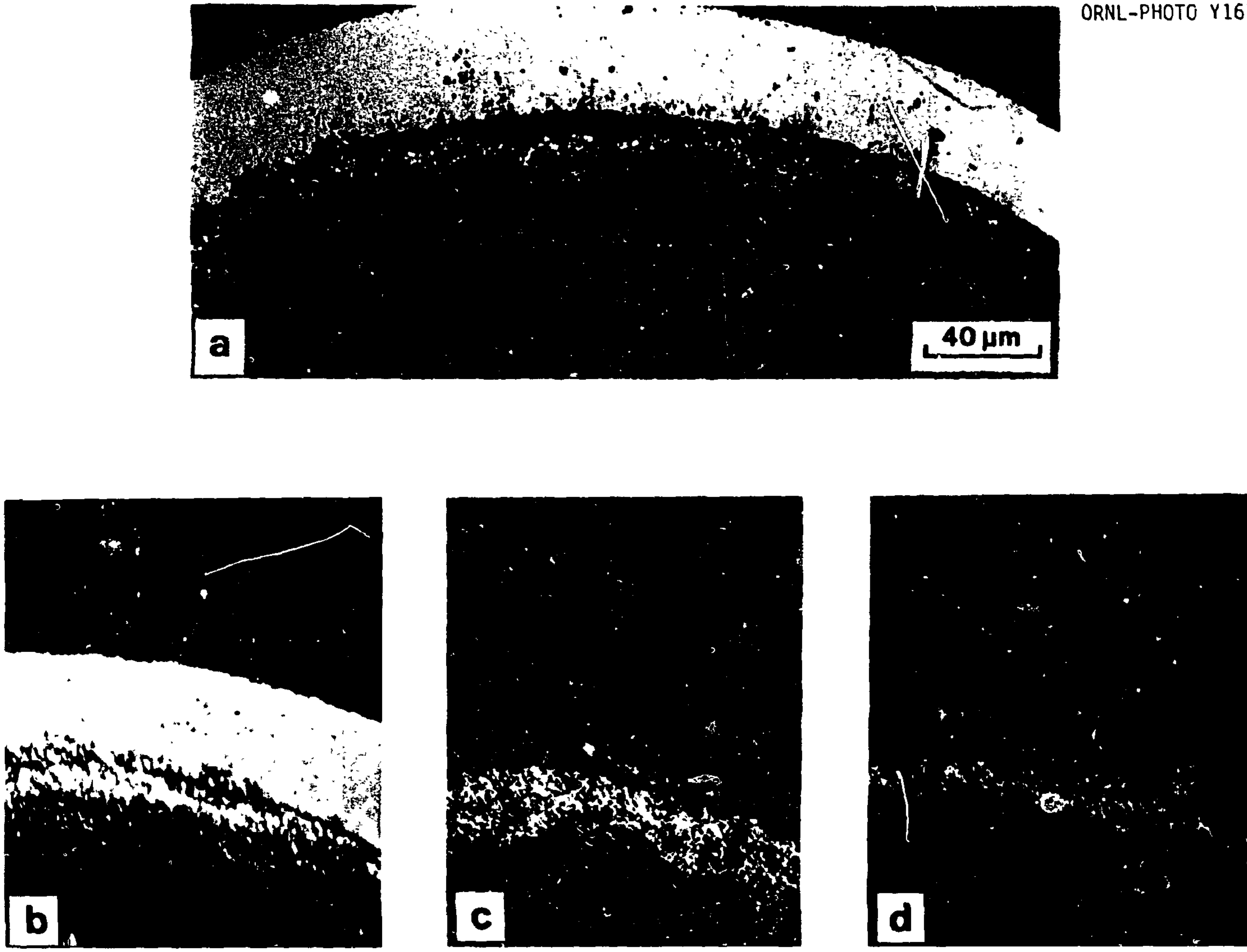

Fig. 4. Triso-coated UO_2 plus Mo-Ru-Pd particle (batch OR-2822) polished to midplane after being heated at 2063 K for 215 h in a 27.8 K/mm temperature gradient. (*a*) Optical micrograph; (*b*) back-scattered electron image of SiC layer; (*c*) Ru L_α x rays; (*d*) Pd L_α x rays.

ORNL-PHOTO Y167289

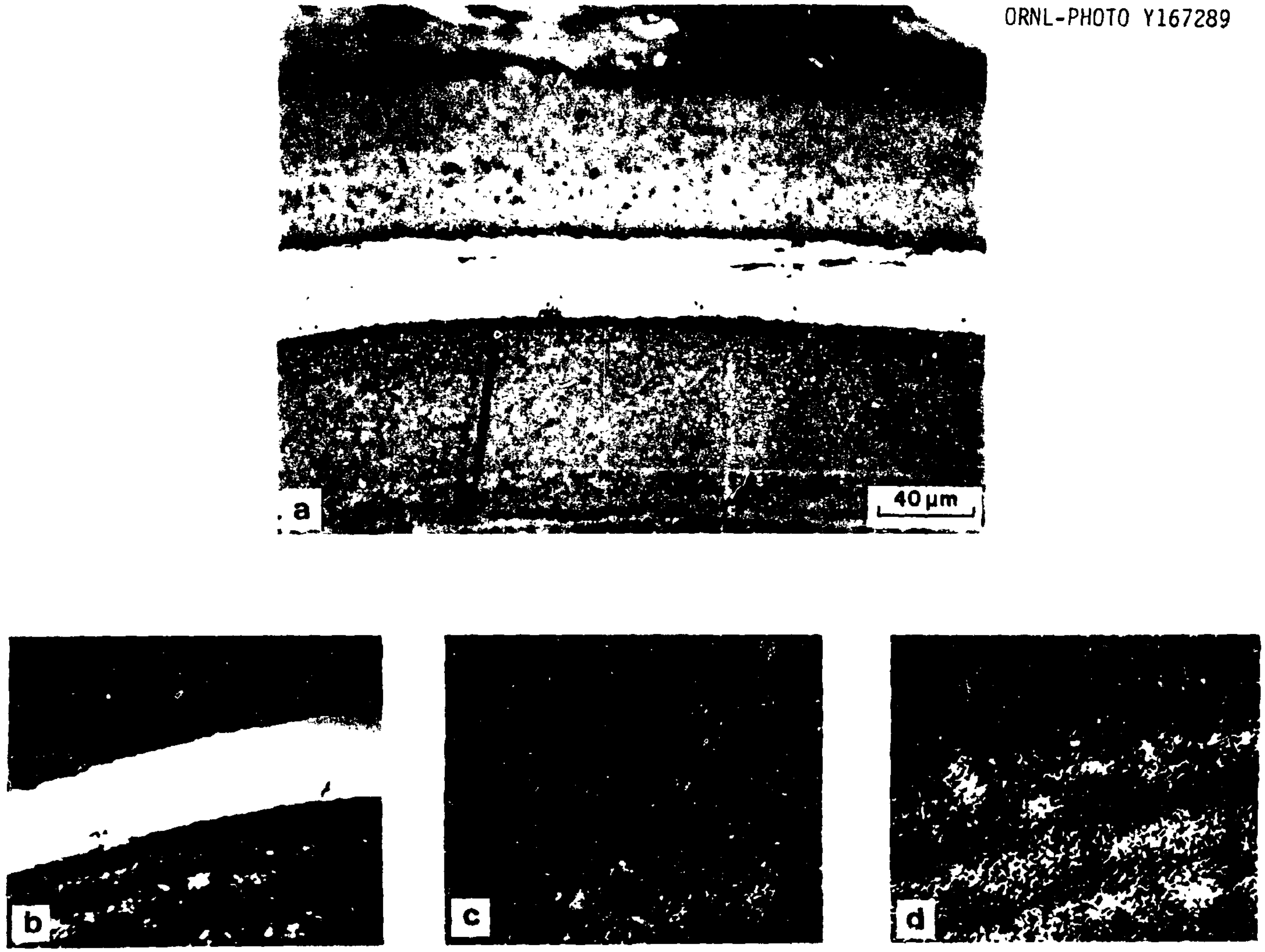

Fig. 5. Triso-coated UO_2 plus Mo-Ru-Rh particle (batch OR-2806) polished to midplane after being heated at 2008 K for 215 h in a 27.8 K/mm temperature gradient. (*a*) Optical micrograph; (*b*) backscattered electron image of SiC layer; (*c*) Ru L_α x rays; (*d*) Rh L_β x rays.

ORNL-PHOTO Y167280

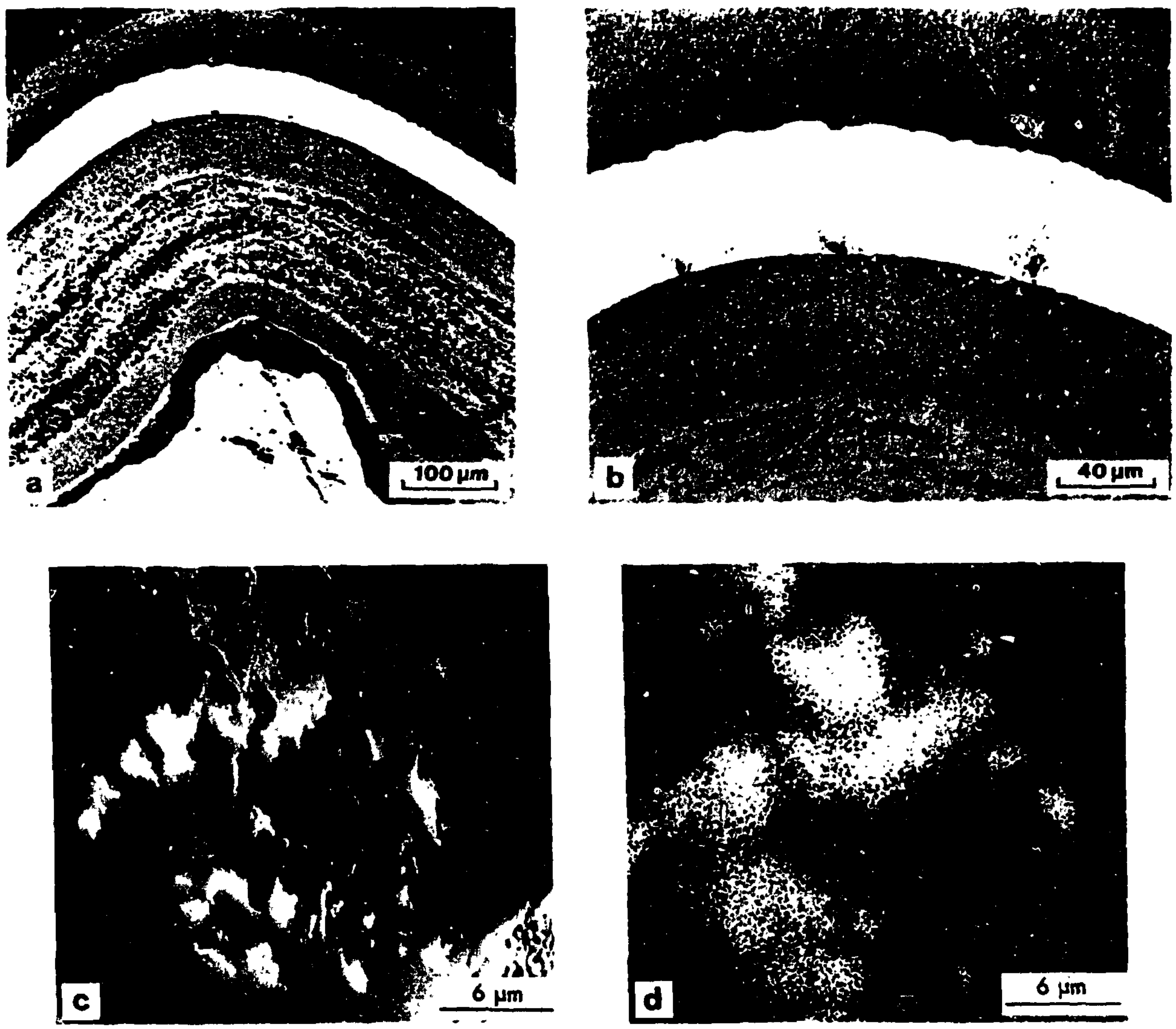

Fig. 6. Triso-coated UO_2 plus Ag particle (batch OR-2775) polished to midplane after heating at 2046 K for 25 h in a 27.8 K/mm temperature gradient. (*a*) Optical micrograph; (*b*) optical micrograph; (*c*) scanning electron micrograph of Ag-SiC interaction zone shown in Fig. 6(*b*); (*d*) Ag L_α x rays of Ag-SiC interaction zone.

determined by dispersive x-ray analysis to lie along the iLTI-SiC interface on the cold side of the particle.

3.3 Triso-Coated Particles Containing UC_2

3.3.1 UC_2 only

Twenty particles of sample 2-10 (batch GA-VSM 6151-00-035) were embedded in a graphite matrix and heat treated at 2173 K for 215 h in a temperature gradient of 27.8 K/mm. No interaction in any of the SiC layers could be detected.

3.3.2 UC_2 plus Mo-Ru-Rh-Pd

Twenty particles of sample 1-2 (batch OR-2773) were embedded in three separate graphite wafers. Each was heat treated in a temperature gradient of 27.8 K/mm - one at 2173 K for 50 h, another at 2073 K for 260 h, and the third at 1773 K for 3528 h. After mounting and polishing the wafers to midplane, we examined them with an optical microscope under bright-field illumination. All of the particles had undergone interaction all the way around the SiC layer. The appearance of the attack differed markedly from the oxide fuel interactions described in Sect. 3.2. Optical micrographs of the SiC layer on the hot and cold sides of a particle heated at 1729 K for 3528 h are shown in Figs. 7(*a*) and 7(*b*). The depth of penetration appeared to be equal, but the size of the second, white phase within the SiC on the cold side was larger than that on the hot side. The difference in attack between the cold and hot sides of a particle was more pronounced in particles heated at higher temperatures. Under the microscope, it became clear at higher magnification that on the hot side of the particle, the second, white phase had extended entirely across the SiC layer. Figure 7(*c*) illustrates complete penetration on the hot side of a particle heated at 2173 K for 50 h. A thorough examination of the SiC layer in a particle heated at 1948 K for 260 h was made using an SEM. On the cold side of the particle, the second, white phase had penetrated 18 μm into the SiC layer, and the nodules were 2 to 3 μm in diameter. On the hot side of the particle, the second, white phase had penetrated all the way through the SiC layer, but those nodules were only 0.5 to 1.0 μm in diameter.

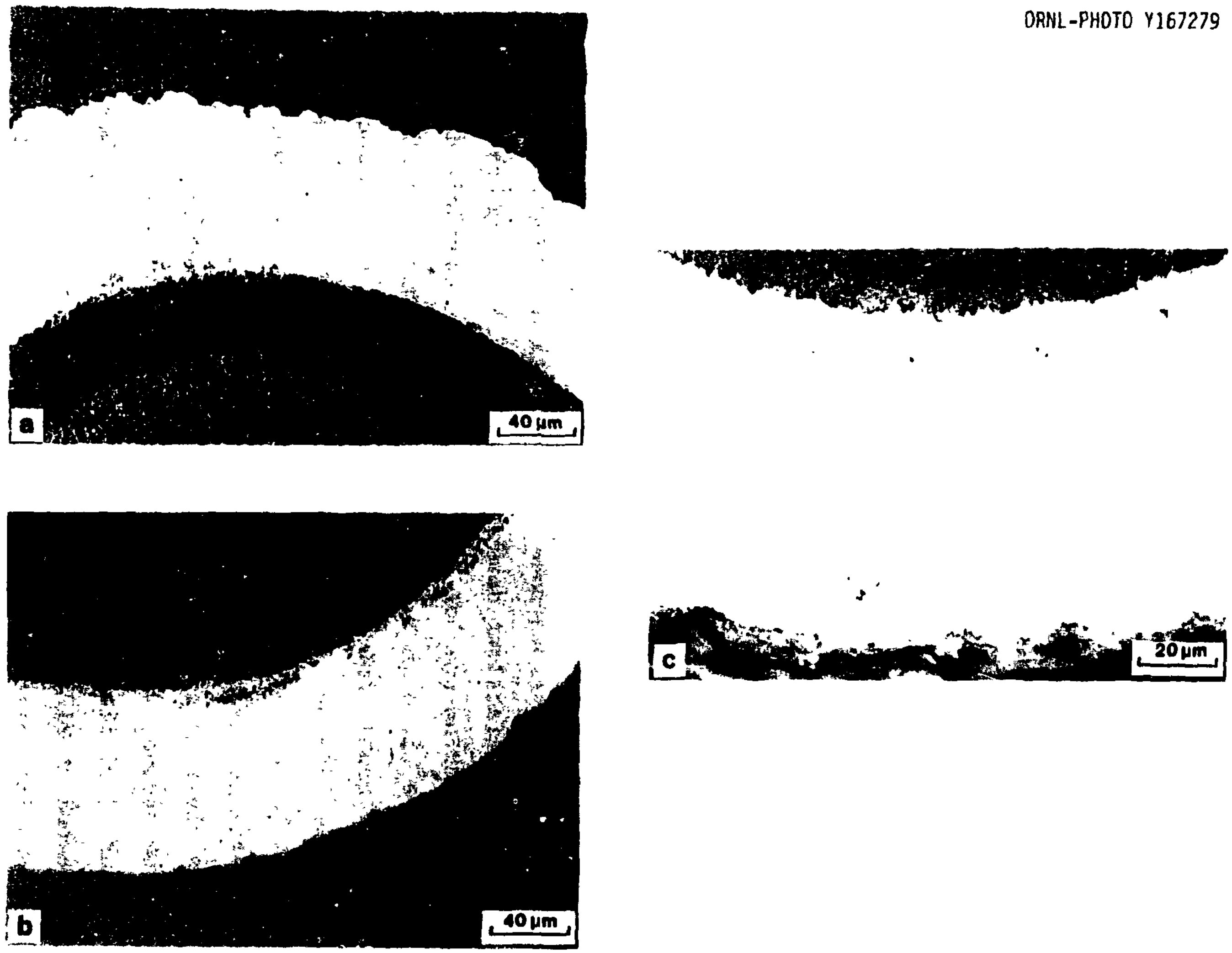

Fig. 7. Optical micrographs of Triso-coated UC_2 plus Mo-Ru-Rh-Pd particles (batch OR-2773) polished to midplane after heat treatment. (*a*) SiC layer on cold side of particle heated at 1729 K for 3528 h; (*b*) SiC layer on hot side of particle heated at 1729 K for 3528 h; (*c*) SiC layer on hot side of particle heated at 2173 K for 50 h. Both particles were heated in a 27.8 K/mm temperature gradient.

All of the particles in the wafer heated to 1773 K for 3528 h were examined with a stereomicroscope under polarized light. The largest area of the second, white phase shown in Fig. 7(*a*) had extended below the surface and had formed nodules much like those described in Sect. 3.2.2, except that there was a change in the color and translucency of the SiC in the vicinity of the nodule. Each nodule was surrounded by a black, cloudy area that was somewhat opaque. Palladium and uranium were detected in these areas by EMP x-ray analyses. As the size of the second, white phase became smaller, the nodules in the SiC became undetectable either by radiography or microscopy. However, the dark opaqueness still existed beyond this white phase, and the depth to which palladium and uranium had reached into the SiC layer could still be measured with the EMP. Sample 1-2 gave good SiC thinning data, but we were unable to precisely identify the interacting species because we could not distinguish between the rhodium and palladium x-ray profiles. When these two elements co-exist, their most prominent x-ray lines overlap.

3.3.3 UC_2 plus Mo-Ru-Pd

Twenty particles of sample 2-1 (batch OR-2809) were embedded in three separate graphite wafers. Each was heat treated in a temperature gradient of 27.8 K/mm - one at 2173 K for 25 h, another at 2173 K for 90 h, and the third at 1873 K for 50 h. Portions of the polished surfaces of all the particles in both wafers heated at 2173 K contained a second, white phase that penetrated all the way through the SiC layers. The wafer heated at 1873 K for 50 h contained some particles whose SiC layers had been penetrated partially and some whose SiC layers had been breached (see Figs. 8 and 9). In the particle heated at 1709 K for 50 h, both palladium and uranium were identified by dispersive x rays to be associated with the white phases in the SiC and at the iLTI-SiC interface. Ruthenium and uranium were found within the iLTI layer and molybdenum only within the kernel.

The particle shown in Fig. 9 was heat treated at 1873 K for 50 h. The SiC layer was breached, and the backscattered electron image [Fig. 9(*a*)] indicated that a portion of the oLTI was filled with heavy

ORNL-PHOTO Y167287

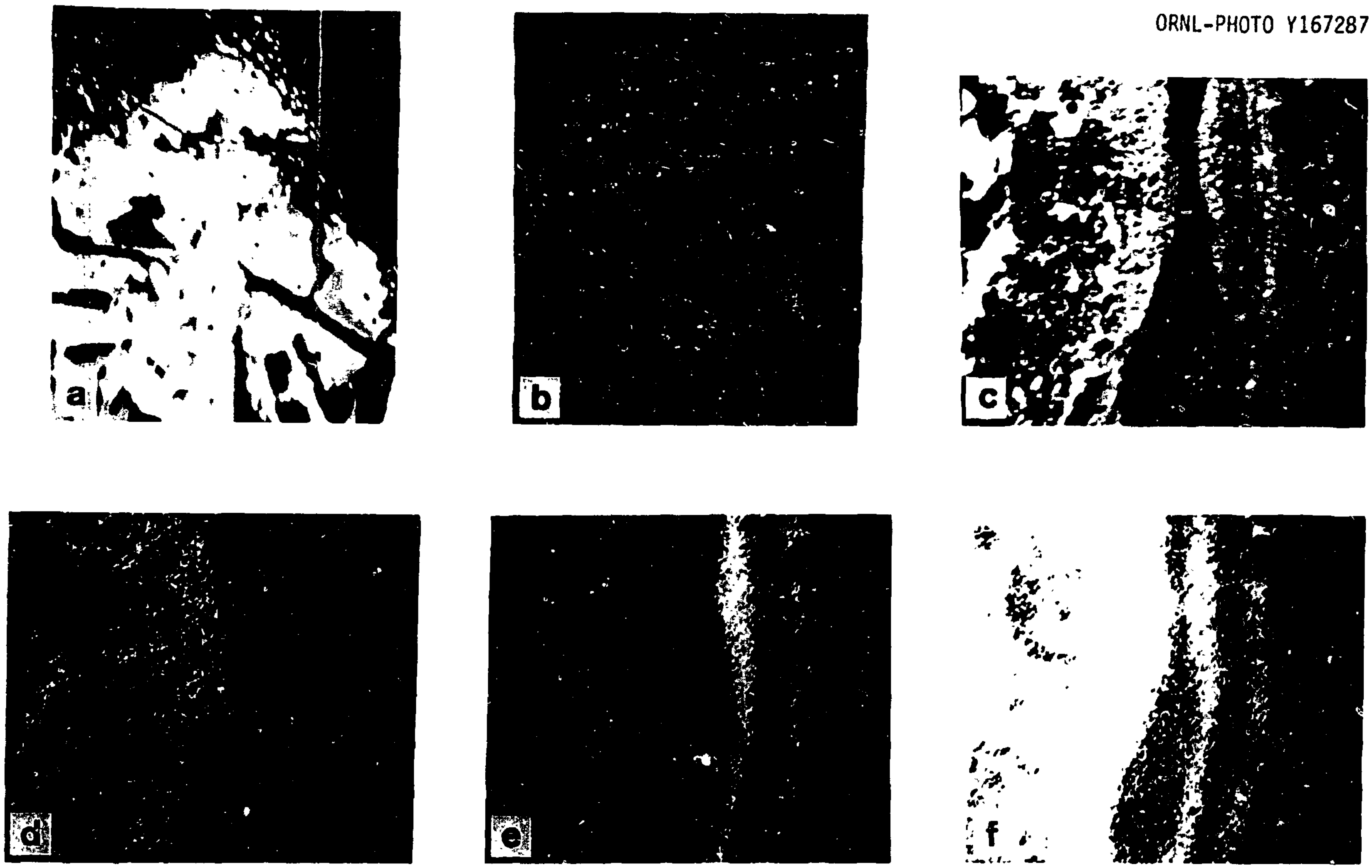

Fig. 8. X-ray displays of Triso-coated UC_2 plus Mo-Ru-Pd particle (batch OR-2809) polished to midplane after being heated at 1790 K for 50 h in a 27.8 K/mm temperature gradient. *(a)* Backscattered electron image of kernel; *(b)* Mo L_α; *(c)* backscattered electron image of SiC layer; *(d)* Ru L_α; *(e)* Pd L_α; *(f)* U M_α.

ORNL-PHOTO Y167288

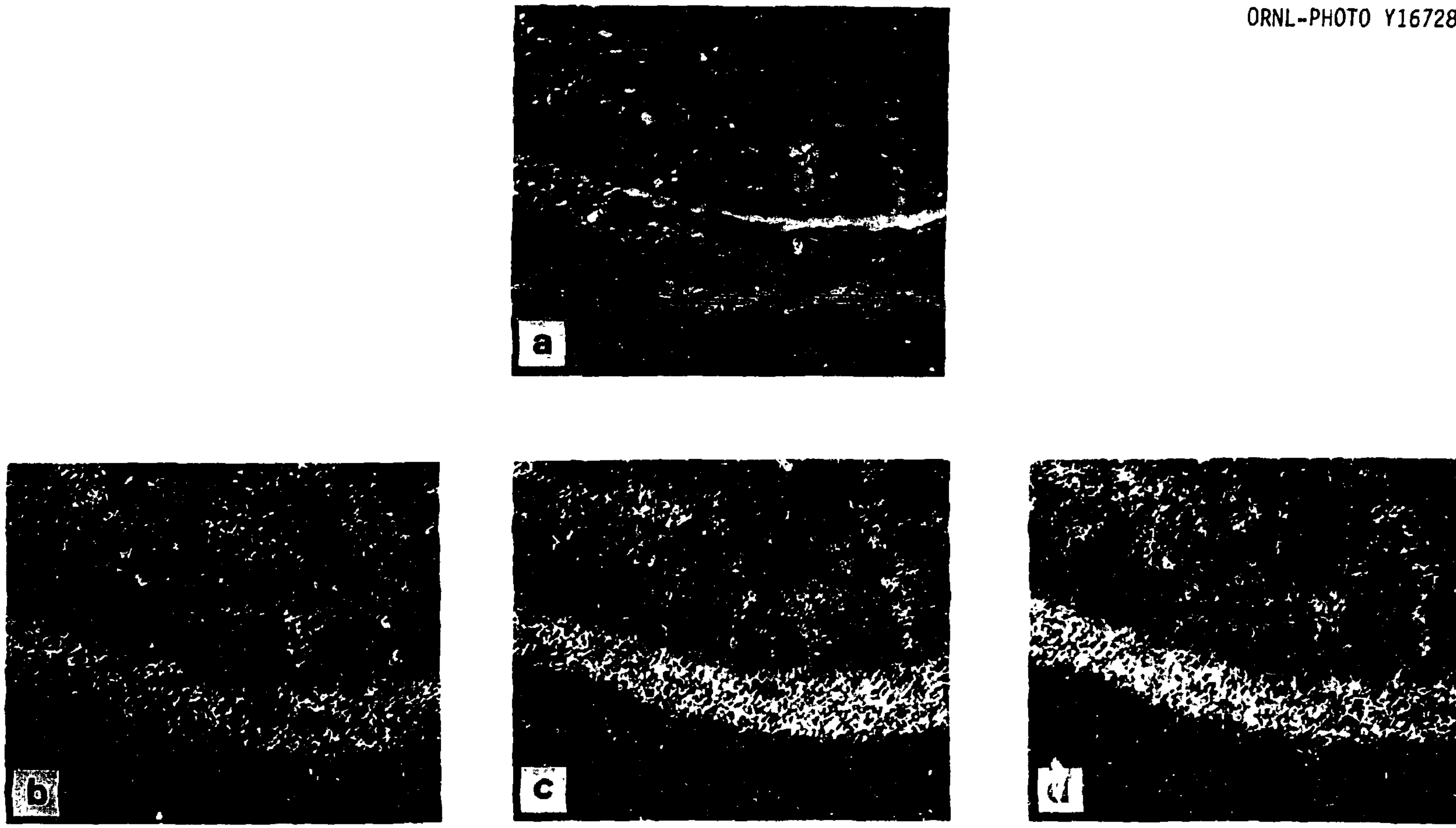

Fig. 9. X-ray displays of Triso-coated UC_2 plus Mo-Ru-Pd particle (batch OR-2809) polished to midplane after being heated at 1873 K for 50 h in a 27.8 K/mm temperature gradient. (*a*) Backscattered electron image of breached SiC layer; (*b*) Ru L_α; (*c*) Pd L_α; (*d*) U M_α.

elements. The x-ray displays in Figs. 9(*b*), 9(*c*), and 9(*d*) identify the heavy elements as ruthenium, palladium, and uranium.

3.3.4 UC_2 plus Mo-Ru-Rh

A graphite wafer filled with 20 particles of sample 2-2 (batch OR-2812) was included in each of the three heat treatments described in Sect. 3.3.3. The heat treatments for these wafers differed only in that the 1873 K test lasted 100 h instead of 50 h. All of the particles heated in the 2173 K test had portions of the SiC layers penetrated by a second, white phase. The particles in the wafer heated at 1873 K for 100 h had some SiC layers that had been penetrated partially and some that had been breached. These can be seen in Figs. 10 and 11. In the particles heated at 1873 K for 100 h, ruthenium, rhodium, and uranium were identified by dispersive x-ray analysis to be associated with the white phases in the SiC and also with the white phase within the iLTI. The particle heated at 1896 K for 100 h had a breached SiC layer, and ruthenium, rhodium, and uranium were found in portions of the oLTI.

3.3.5 UC_2 plus Mo-Ru-Pd-La

A graphite wafer filled with 20 particles of sample 2-2 (batch OR-2814) was included in each of the three heat treatments described in Sect. 3.3.3. With some lanthanum added to the UC_2-Mo-Ru-Pd kernel, the SiC interaction was more severe than the reaction with the UC_2-Mo-Ru-Pd kernel, and the photomicrographs of the reaction zones seemed to show more contrast. After heat treatment at 1709 K for 50 h, some of the metals had penetrated the iLTI layer and concentrated at several points along the iLTI-SiC interface [Figs. 12(*a*) and 12(*b*)]. At these points, the structure and appearance of the iLTI layer had changed; the light gray, dense pyrolytic carbon had changed to a darker gray area flecked with a white phase. No optical activity in these areas could be seen under polarized light.

Immediately adjacent to these metal concentration points, a second, white phase had begun to penetrate the SiC layer. Ruthenium, palladium,

ORNL-PHOTO Y167286

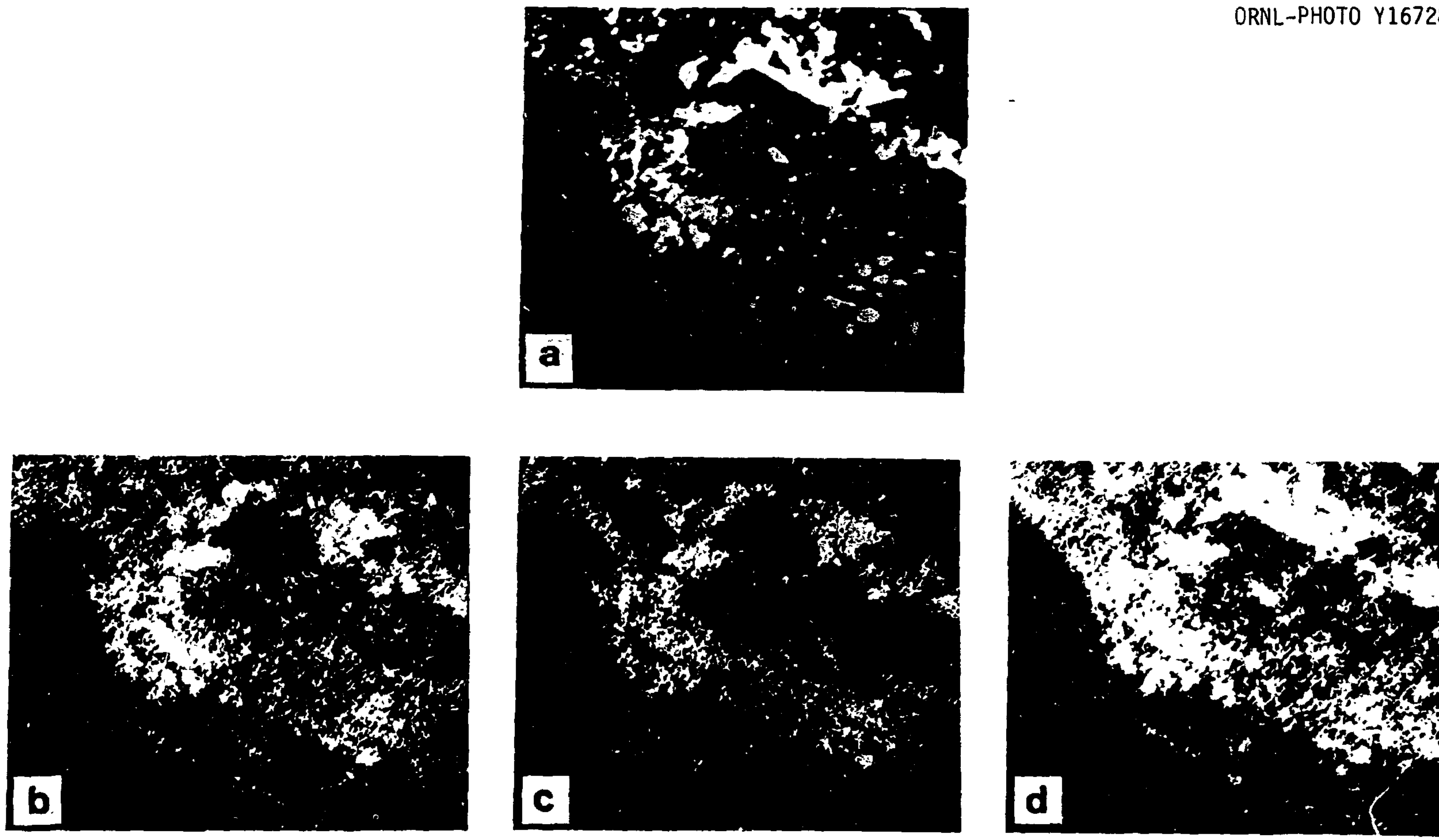

Fig. 10. X-ray displays of Triso-coated UC_2 plus Mo-Ru-Rh particle (batch OR-2812) polished to midplane after being heated at 1873 K for 100 h in a 27.8 K/mm temperature gradient. (*a*) Backscattered electron image of SiC layer; (*b*) Ru L_α; (*c*) Rh L_β; (*d*) U M_α.

ORNL-PHOTO Y167284

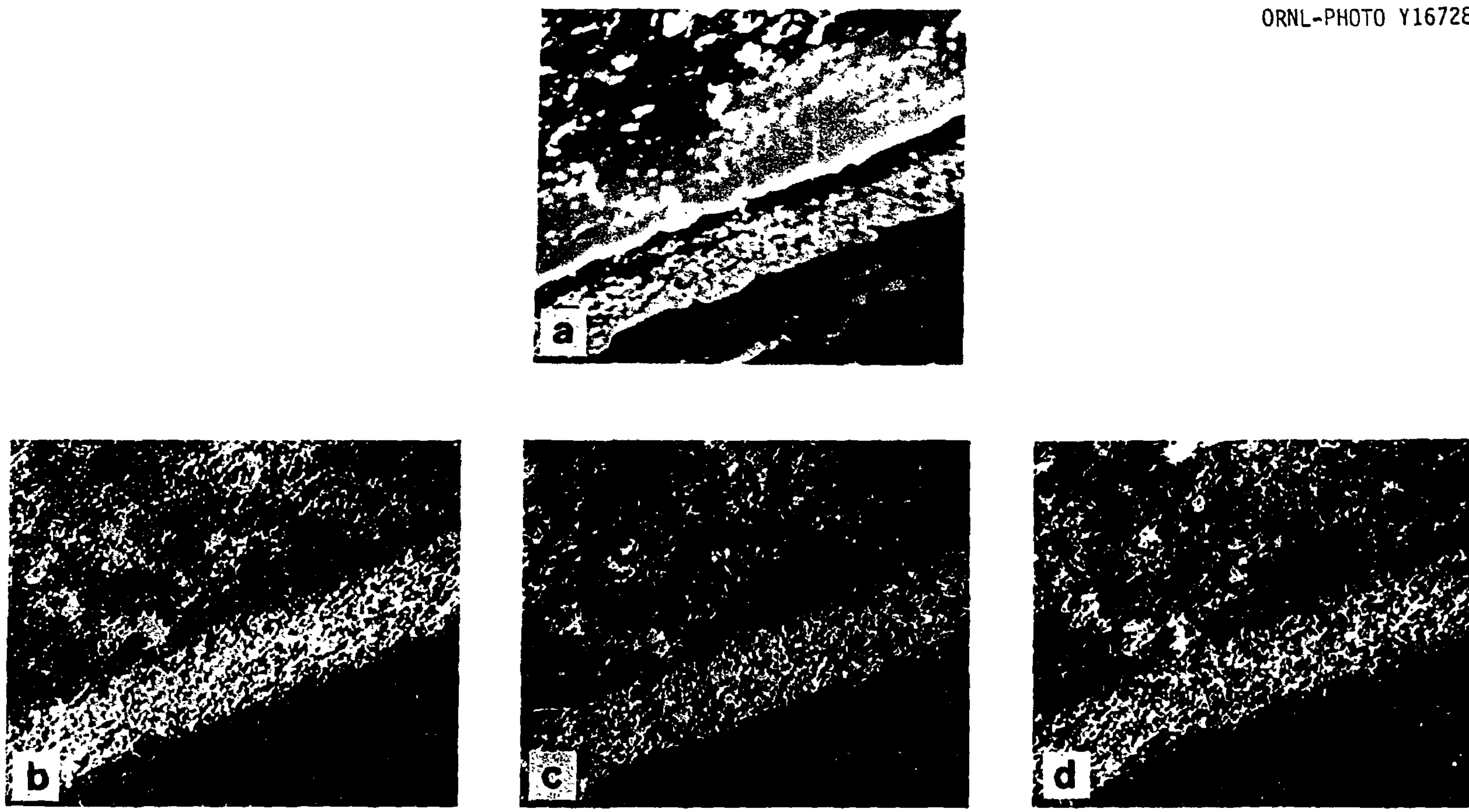

Fig. 11. X-ray displays of Triso-coated UC_2 plus Mo-Ru-Rh particle (batch OR-2812) polished to midplane after being heated at 1896 K for 100 h in a 27.8 K/mm temperature gradient. (*a*) Backscattered electron image of breached SiC layer; (*b*) Ru L_α; (*c*) Rh L_β; (*d*) U M_α.

ORNL-PHOTO Y167277

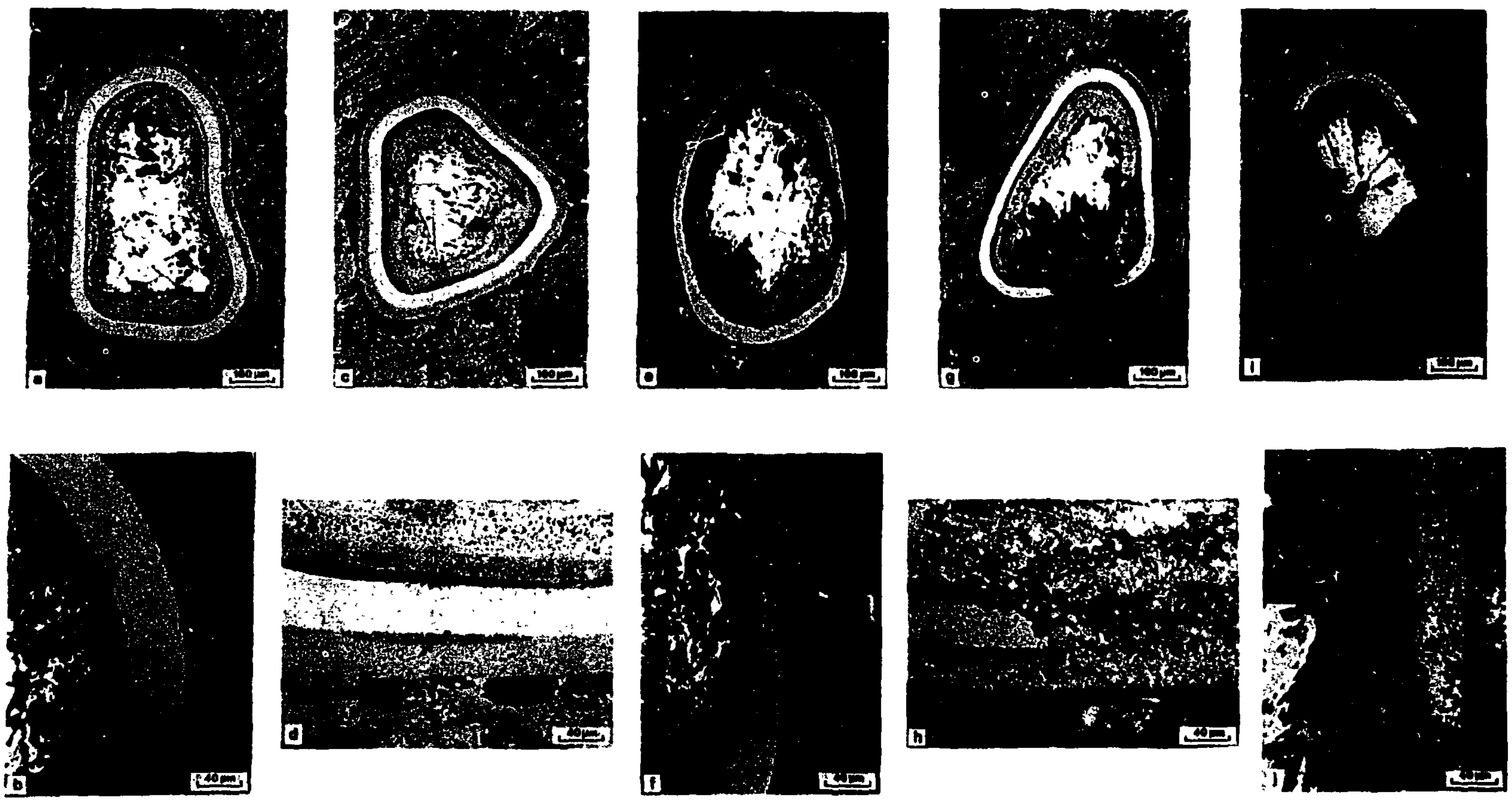

Fig. 12. Optical micrographs of UC_2 plus Mo-Ru-Pd-La particles (batch OR-2814) polished to midplane after being heated. (*a*) 1709 K for 50 h; (*b*) same particle as shown in (*a*); (*c*) 1827 K for 50 h; (*d*) same particle as shown in (*c*); (*e*) 1859 K for 50 h; (*f*) same particle as shown in (*e*); (*g*) 1934 K for 25 h; (*h*) same particle as shown in (*g*); (*i*) 2098 K for 90 h; (*j*) same particle as shown in (*i*). All the particles were heated in a 27.8 K/mm temperature gradient. The cold side of each particle is oriented at the top of each photographic image.

and uranium were identified by dispersive x-ray analysis to be associated with the white phase within the darker gray areas at the SiC-iLTI interface, and palladium and uranium in the white phase in the SiC layer. The particle shown in Figs. 12(*c*) and 12(*d*) was heated at 1827 K for 50 h. The metals breached the SiC layer and began to enter the oLTI layer. The appearance and structure of this area had changed; it appeared darker and less dense. Palladium, ruthenium, and uranium were found within the area. The interior surface of the SiC, opposite where the metals entered the oLTI, showed signs of erosion. In Figs. 12(*e*) and 12(*f*), it can be seen that the integrity of the SiC layer, which was heated at 1859 K for 50 h, had been destroyed. The metals appeared to have seeped along most of the SiC-oLTI interface and then into the oLTI layer itself. Palladium, ruthenium, and uranium were still within the oLTI. Figures 12(*g*) and 12(*h*) show a particle heated at 1934 K for 25 h. The heavy metals completely penetrated the oLTI, and parts of the SiC layer were consumed. Finally, in Figs. 12(*i*) and 12(*j*), a particle is shown that was heated at 2098 K for 90 h. Most of the Triso coating had disintegrated. Over half of the ends of the remaining SiC layer was the second, white phase, containing mainly uranium with a little silicon. The darker phase - the remaining SiC - contained mainly silicon; a little ruthenium, palladium, and uranium were identified in the white material accumulated in the destroyed oLTI. No lanthanum was found in any of the heat treated particles in Figs. 12(*a*) through 12(*j*).

3.4 Triso-Coated Particles Containing UO_2/UC_2 Mixtures Plus Mo, Rh, and Pd

3.4.1 65% UO_2/35% UC_2 plus Mo-Ru-Pd

Twenty particles of sample 2-7 (batch OR-2807) were embedded in a graphite matrix and heat treated at 2173 K for 215 h in a temperature gradient of 27.8 K/mm. Some SiC interaction occurred in several of the particles. One such particle heated at 2025 K is shown in Fig. 13. Dispersive x-ray analysis identified both palladium and uranium, but not ruthenium, within the SiC layer.

ORNL-PHOTO Y167281

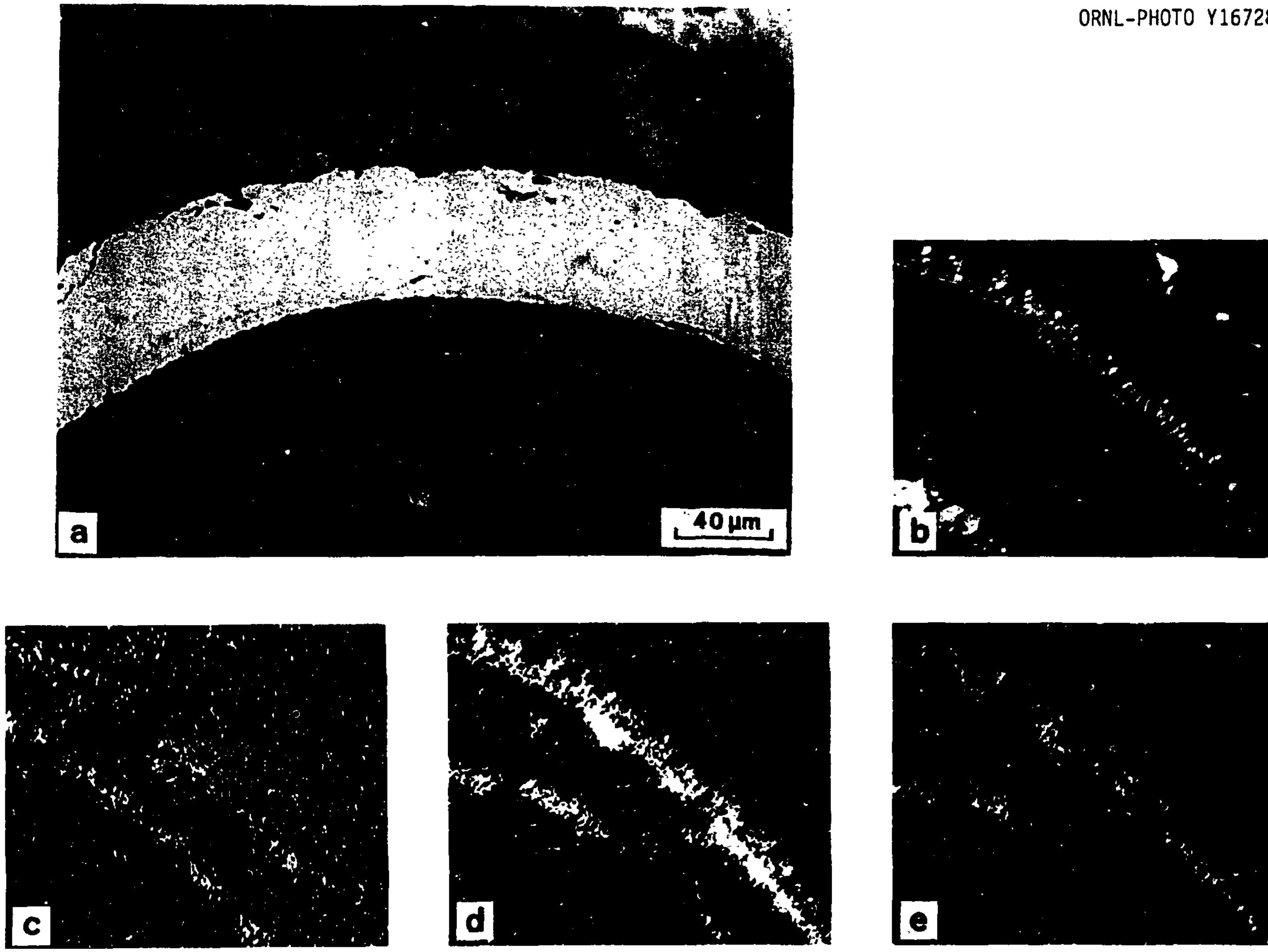

Fig. 13. Triso-coated 65% UO_2/35% UC_2 plus Mo-Ru-Pd particle (batch OR-2807) polished to midplane after being heated at 2025 K for 215 h in a 27.8 K/mm temperature gradient. (*a*) Optical micrograph; (*b*) backscattered electron image of SiC layer; (*c*) Ru L_α x rays; (*d*) Pd L_α x rays; (*e*) U M_α x rays.

3.4.2 90% UO_2/10% UC_2 plus Mo-Ru-Pd

Twenty particles of sample 2-6 (batch OR-2823) were embedded in a graphite matrix and heat treated at 2173 K for 215 h in a temperature gradient of 27.8 K/mm. Interaction with SiC occurred in several of the particles. The particle shown in Fig. 14 was heated at 2123 K. Like the particles reported in Sect. 3.4.1, palladium and uranium, but not ruthenium, were identified within the SiC layer.

3.5 SiC Thinning Rates

The SiC thinning rates were obtained from samples 1-2, 2-4, 2-5, 2-6, and 2-7, but not from any of the defective samples. The rate of SiC thinning as a function of temperature for the UO_2, UC_2, and UO_2/UC_2 Triso-coated particles that contained palladium is plotted in Fig. 15. The SiC thinning rate data for Triso-coated UO_2 that contained rhodium, but no palladium, are plotted in Fig. 16. The quantitative results from which the thinning rates were calculated are listed in Table 5.

4. DISCUSSION

4.1 The SiC Thinning Rate

The two sets of confidence limits shown in Figs. 15 and 16 are from a recent General Atomic Company (GAC) report[18] and need to be revised partially in view of the present results. The confidence limits for data above 1673 K are undoubtedly for the interaction of rare-earth carbides with SiC in particles containing UC_2 kernels. Reviewing this briefly, GAC obtained their data by irradiating HEU UC_2 fuel particles and then heating them in a temperature gradient in a laboratory furnace.[1] The interaction was measured radiographically, and no attempt was made to identify the interacting species. However, in parallel ORNL work,[10] Triso-coated rare earth-carbide kernels were heated in a temperature gradient, and the radiographically determined SiC thinning rates all fell within the GAC 95% confidence limits. Thus the SiC thinning rates above 1673 K measured from radiographs by GAC were apparently due to rare-earth

ORNL-PHOTO Y167282

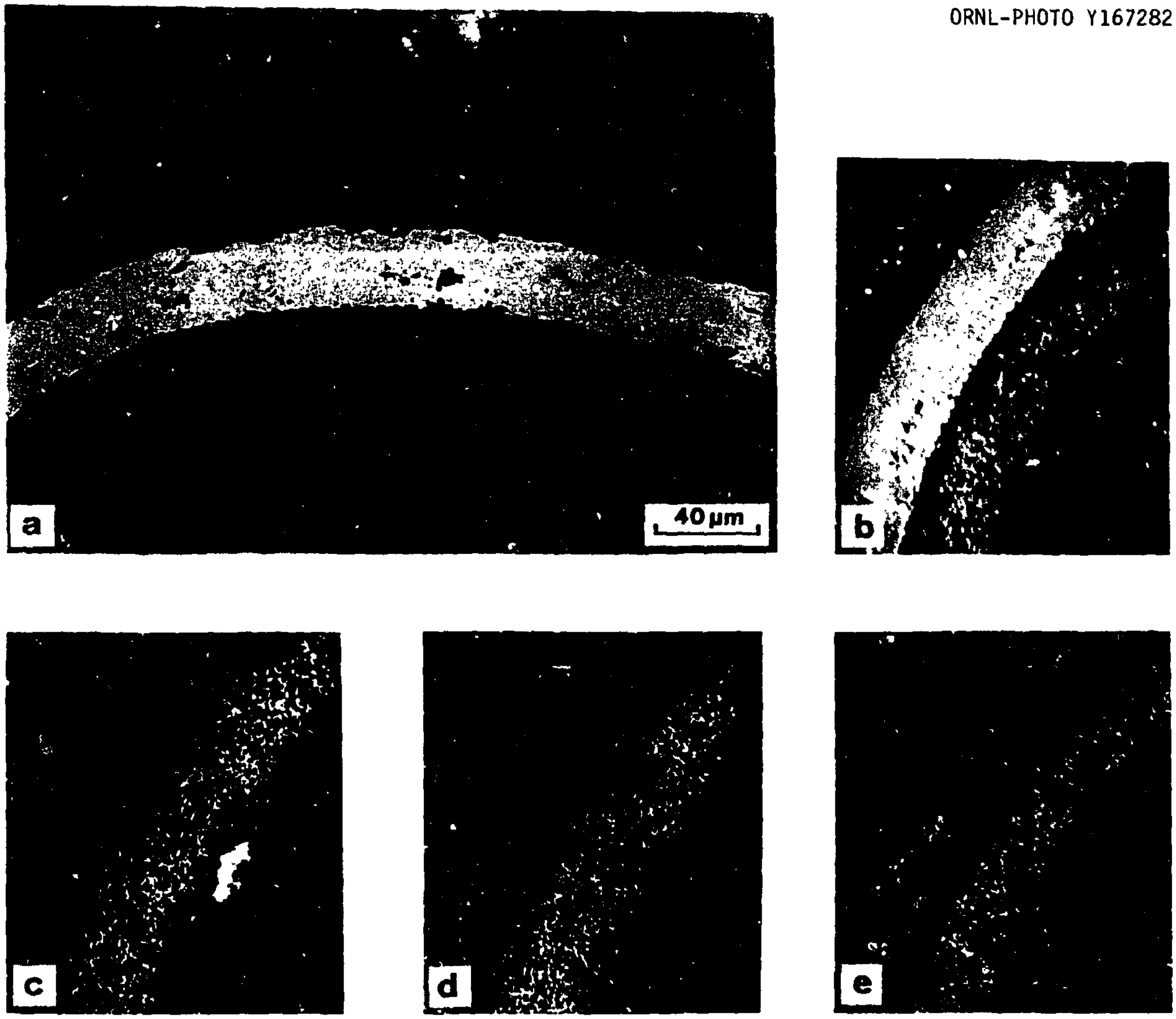

Fig. 14. Triso-coated 90% UO_2/10% UC_2 plus Mo-Ru-Pd particle (batch OR-2823) polished to midplane after being heated at 2123 K for 215 h in a 27.8 K/mm temperature gradient. (*a*) Optical micrograph; (*b*) backscattered electron image of SiC layer; (*c*) Ru L_α x rays; (*d*) Pd L_α x rays; (*e*) U M_α x rays.

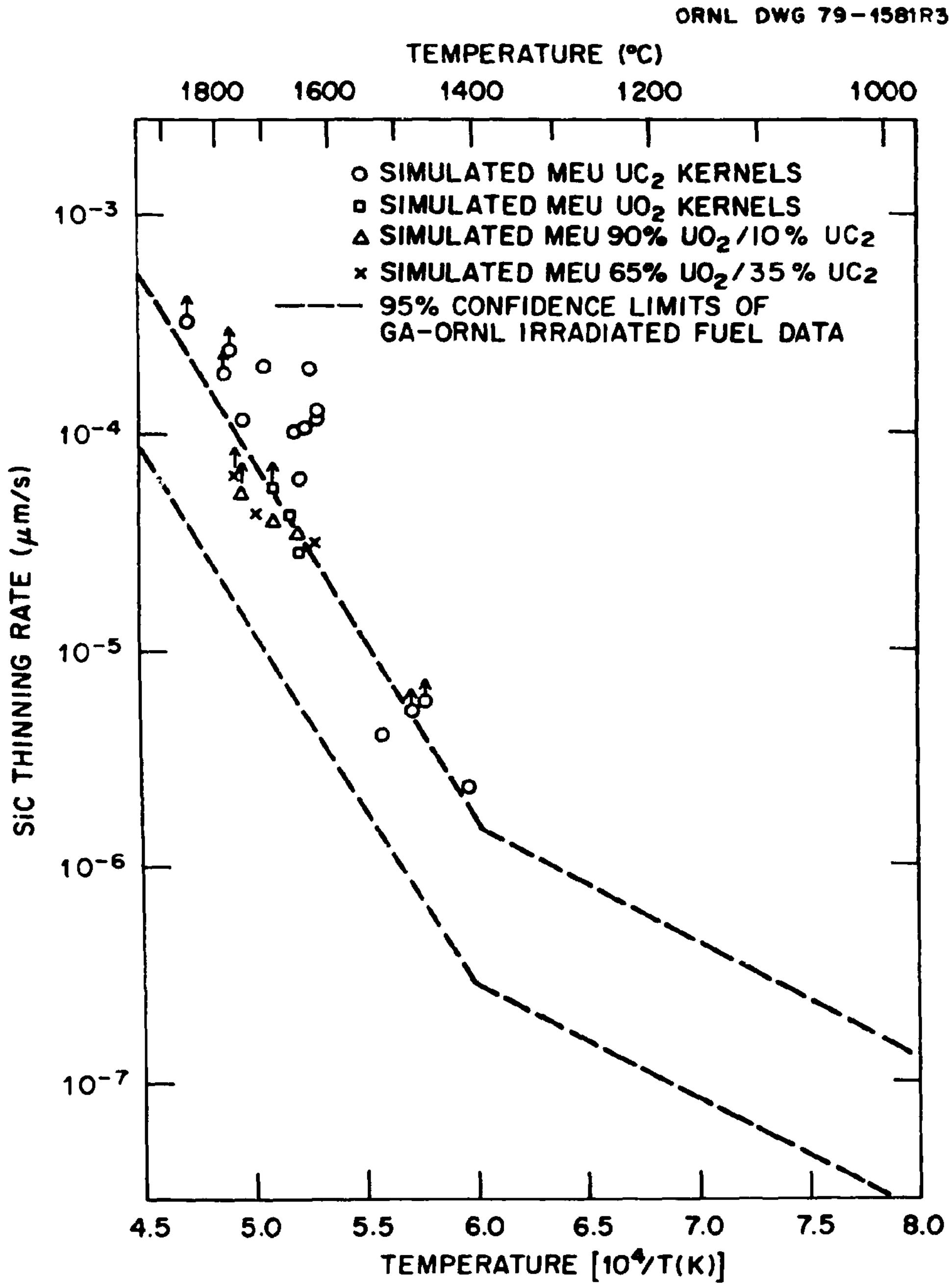

Fig. 15. SiC thinning rate for simulated, palladium-containing Triso-coated particles versus reciprocal temperature. The points with arrows above them indicate complete penetration of the SiC layer sometime during heat treatment. All of the particles were heated in a 27.8 K/mm temperature gradient.

ORNL DWG 79-1580R

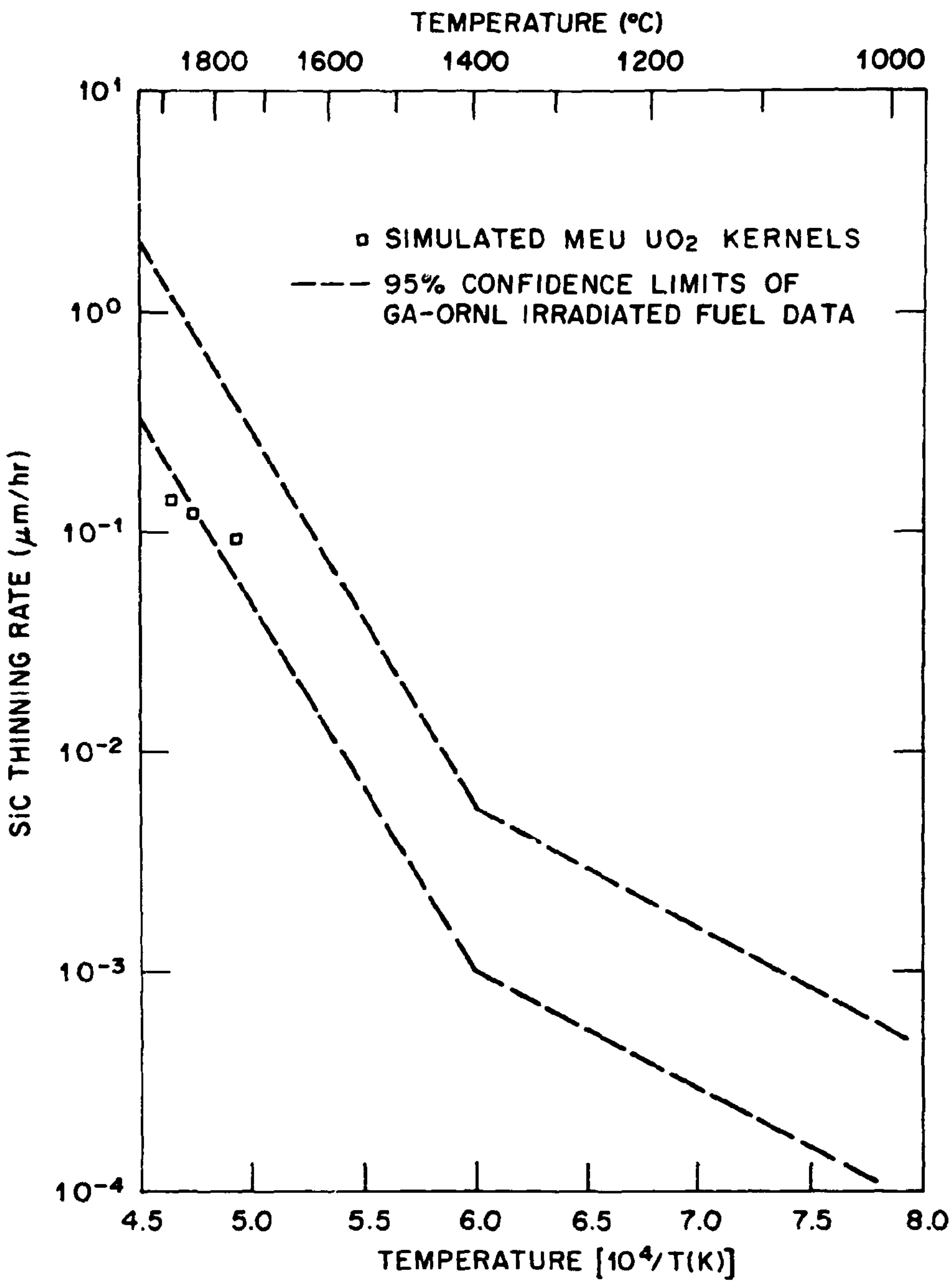

Fig. 16. SiC thinning rate for Triso-coated UO_2 plus Mo-Ru-Rh particles versus reciprocal temperature. All of the particles were heated in a 27.8 K/mm temperature gradient.

Table 5. Quantitative fission product–SiC interaction results

Sample	Temperature (K)	Time (s)	Penetration (μm)
1-2[a]	2174	1.8×10^5	58[f]
1-2	2169	1.8×10^5	50[f]
1-2	2119	1.8×10^5	54[f]
1-2	2045	1.8×10^5	34
1-2	2033	1.8×10^5	43
1-2	2012	1.8×10^5	21
1-2	1976	1.8×10^5	37
1-2	1923	1.8×10^5	18
1-2	1905	1.8×10^5	19
1-2	1887	1.8×10^5	23
1-2	1887	1.8×10^5	21
1-2	1792	1.27×10^7	51
1-2	1751	1.27×10^7	65[f]
1-2	1730	1.27×10^7	73[f]
1-2	1675	1.27×10^7	29
2-4[b]	1961	7.74×10^5	43[f]
2-4	1934	7.74×10^5	20
2-4	1919	7.74×10^5	28
2-6[c]	2020	7.74×10^5	40[f]
2-6	1961	7.74×10^5	30
2-6	1923	7.74×10^5	26
2-7[d]	2020	7.74×10^5	49[f]
2-7	1988	7.74×10^5	33
2-7	1894	7.74×10^5	24.5
2-5[e]	2151	7.74×10^5	30
2-5	2110	7.74×10^5	26
2-5	2024	7.74×10^5	20

[a] UC_2 plus Mo-Ru-Rh-Pd (batch OR-2773).

[b] UO_2 plus Mo-Ru-Pd (batch OR-2822).

[c] 90% UO_2/10% UC_2 plus Mo-Ru-Pd (batch OR-2823).

[d] 65% UO_2/35% UC_2 plus Mo-Ru-Pd (batch OR-2807).

[e] UO_2 plus Mo-Ru-Rh (batch OR-2806).

[f] Interaction has penetrated SiC layer.

interactions with SiC. Below 1673 K, the data were determined metallographically at GAC and ORNL from polished irradiated particles in which the interacting species was identified as palladium.

The present investigation from 1673 to 2173 K revealed that radiography cannot be used to measure SiC thinning in either UC_2 plus Mo-Ru-Rh-Pd, UO_2 plus Mo-Ru-Pd, UO_2 plus Mo-Ru-Rh, or UO_2/UC_2 plus Mo-Ru-Pd particles. Unlike the rare-earth interaction with SiC, which occurred only on the cold side of the particles and resulted in a sharp interface, the SiC-Pd and SiC-Rh interactions occurred anywhere within the particle. The SiC thinning rate was faster on the hot side than it was on the cold side of the particle. Unfortunately, the interface on the hot side was diffuse and could not be distinguished clearly in a radiograph. At 2173 K, however, the penetration front on the hot side could be seen easily by metallographic technique. Nodules containing either palladium, rhodium, or palladium with uranium were distributed throughout the SiC layer. They could be seen at the polished surface in bright-field illumination, or under the surface in polarized or oblique light, since unirradiated SiC is translucent.

As the experimental temperature decreased from 2173 K, the nodules in the SiC became smaller and smaller until they could no longer be detected with a microscope. However, metal penetration into the SiC could still be measured with an SEM. The thinning rate data for palladium above 1673 K are clearly higher than those for the rare-earth carbides (Fig. 15) and are replotted in Fig. 17. The three sets of 95% confidence limits are for the ORNL laboratory data above $\sim$1673 K, the ORNL in-reactor data below $\sim$1673 K, and all the ORNL data. It is unclear at the present time which set of limits should be used.

The results shown in Figs. 15, 16, and 17 indicate that (1) above 1673 K, the rate of SiC thinning due to SiC-Pd interaction is 3 to 5 times greater than SiC thinning due to rare-earth interaction with SiC, (2) the SiC thinning rate due to SiC-Pd interaction is not influenced by kernel composition, and (3) the rate of SiC thinning due to fission product interaction occurs in the order palladium > rare earths > rhodium.

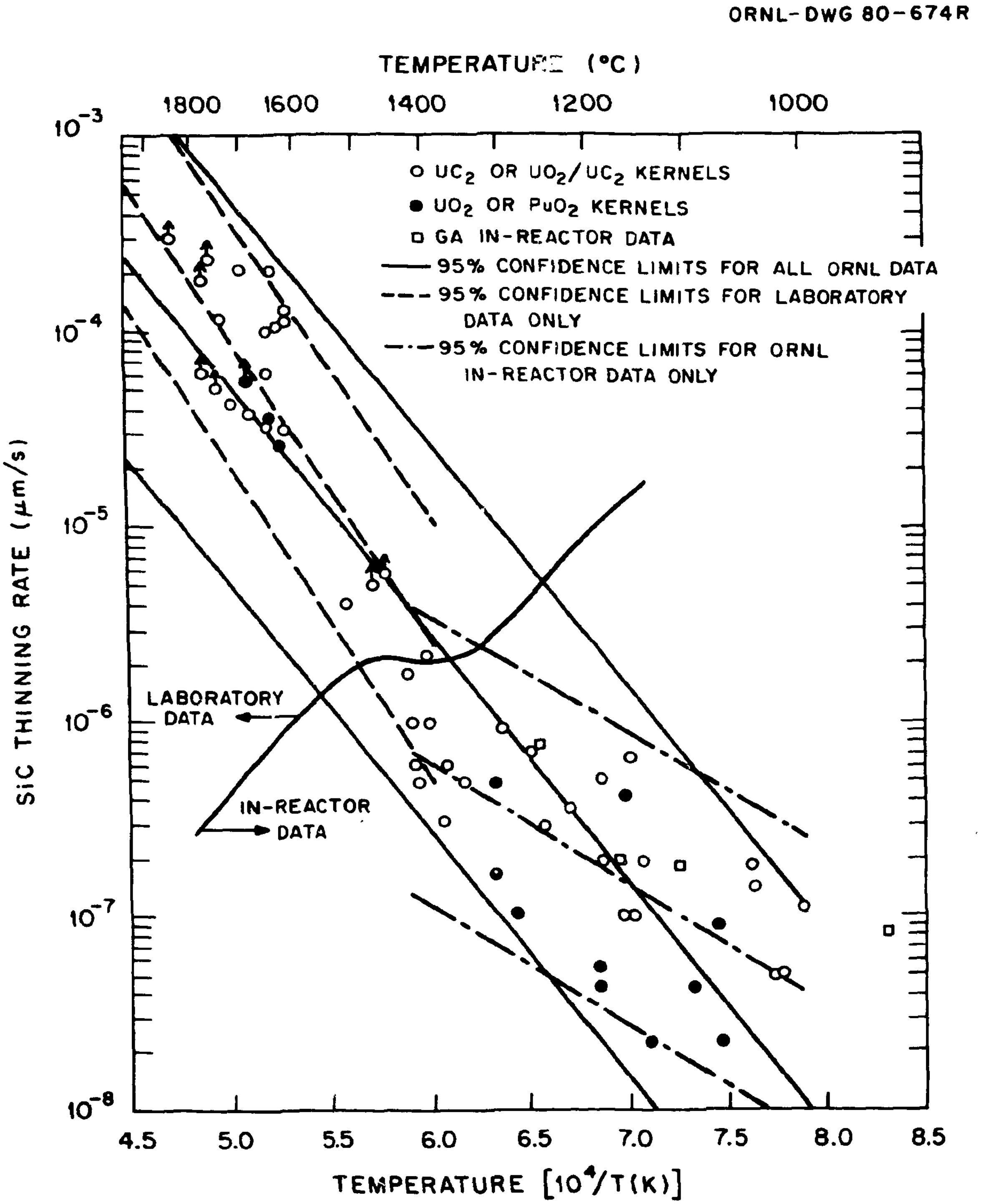

Fig. 17. SiC thinning rate due to palladium-SiC interactions versus reciprocal temperature. Data were obtained from a variety of Triso-coated particles heat treated in the laboratory and in the reactor.

4.2 Fuel—Fission Product Chemistry

In order to attempt an understanding of the fission product interaction with the SiC, it is necessary to examine the chemical behavior within the particles. As mentioned in Sect. 2.1, the noble metals Ru, Tc, Rh, Pd, and part of the Mo form homogeneous alloy inclusions within the UO_2.[12] The rest of the molybdenum may exist as an oxide solid solution with the UO_2. Silver and cadmium do not form oxides at the fuel operating conditions. In UC_2 fuel, the noble metals all form compounds.[19] Palladium can form the compound UPd_3. Ruthenium and rhodium can form the carbides U_2RuC_2 and U_2RhC_2, which form a solid solution, and $URu_3C_{0.7}$ and $URh_3C_{0.1}$, which also form a solid solution. Molybdenum can exist either as $UMoC_2$ or Mo_2C. Neither silver nor cadmium forms carbides.

With so many possible chemical compounds within Triso-coated UC_2 particles during irradiation, one needs to determine the equilibrium composition. This was done with SOLGASMIX-PV, a computer program that calculates thermodynamic equilibrium compositions in complex chemical systems.[20] Table 6 lists the thermodynamic values used for all the species considered. The calculated results list both the equilibrium composition and the vapor pressure of each chemical species. These are plotted as a function of temperature in Figs. 1 and 18. The most notable changes in the equilibrium composition between Triso-coated UO_2 and UC_2 fuel is that in UO_2, the noble metal fission products exist as a homogeneous metallic alloy. In UC_2 almost all of the palladium exists as UPd_3, most of the ruthenium exists as U_2RuC_2 below 1500°C and as $URu_3C_{0.7}$ above 1500°C, and the rhodium exists as U_2RhC_2 below 1500°C and as $URh_2C_{0.1}$ above 1500°C. The vapor pressures of the noble metals in UO_2 are all higher by one or two orders of magnitude than in UC_2, depending on temperature. The uranium vapor pressure within Triso-coated UC_2 particles is comparable with the vapor pressure of some of the other fission products, but in Triso-coated UO_2 particles the uranium vapor pressure is insignificant. Molybdenum has a very low vapor pressure in both the UO_2 and UC_2 fuel particles. In either Triso-coated UO_2 or UC_2 particles, the vapor pressures of silver and cadmium may be as high as that in equilibrium with the condensed elements.

Table 6. Thermodynamic values

Species[a]	Temperature (K)	ΔH_f^o (kJ/mol)	ΔS_f^o (J/mol-K)	Reference
(C)		715.3	156.9	21
(C_2)		825.7	189.5	21
(C_3)		780.6	187.4	21
(Mo)		658.2	153.2	22
(Pd)		376.2	129.2	22
(Rh)		553.1	154.2	22
(Ru)		651.5	157.9	22
(U)		523.0	149.4	22
(UC_2)		642.3	161.5	21
<UC>		-109.9	-0.83	21
<U_2C_3>		-201.1	+11.1	21
<Mo_2C>		-46.0	+2.64	23
<$UMoC_2$>	1000-1200	-274.4	-90.0	24
<UPd_3>	1373-1773	-379.1	-54.8	25
<SiC> (alpha)		-71.6	-8.08	26
<SiC> (beta)		-73.2	-7.95	26
<U_3Si>		-92.1	-2.34	23
<U_3Si_2>		-170.7	+8.95	23
<USi>		-84.5	-2.59	23
<U_3Si_5>		-354.4	-13.60	23
<USi_2>		-129.7	-6.11	23
<USi_3>		-130.5	-0.50	23
<Pd_3Si>		-92.1	0	27
<Pd_2Si>		-87.9	0	27
<PdSi>		-79.5	0	27
[U_2RhC_2]	1000-1200	-303.4	-32.9	28
[U_2RuC_2]	1000	-334.7	-32.9	29
[$URh_3C_{0.1}$]	870-1100	-238.5	+23.0	30
[$URu_3C_{0.7}$]	860-1070	-222.2	+29.3	31

[a]The following notation is used: ( ), gaseous state; < >, compound in solid state; [ ], solid solution.

ORNL-DWG 79-10944R

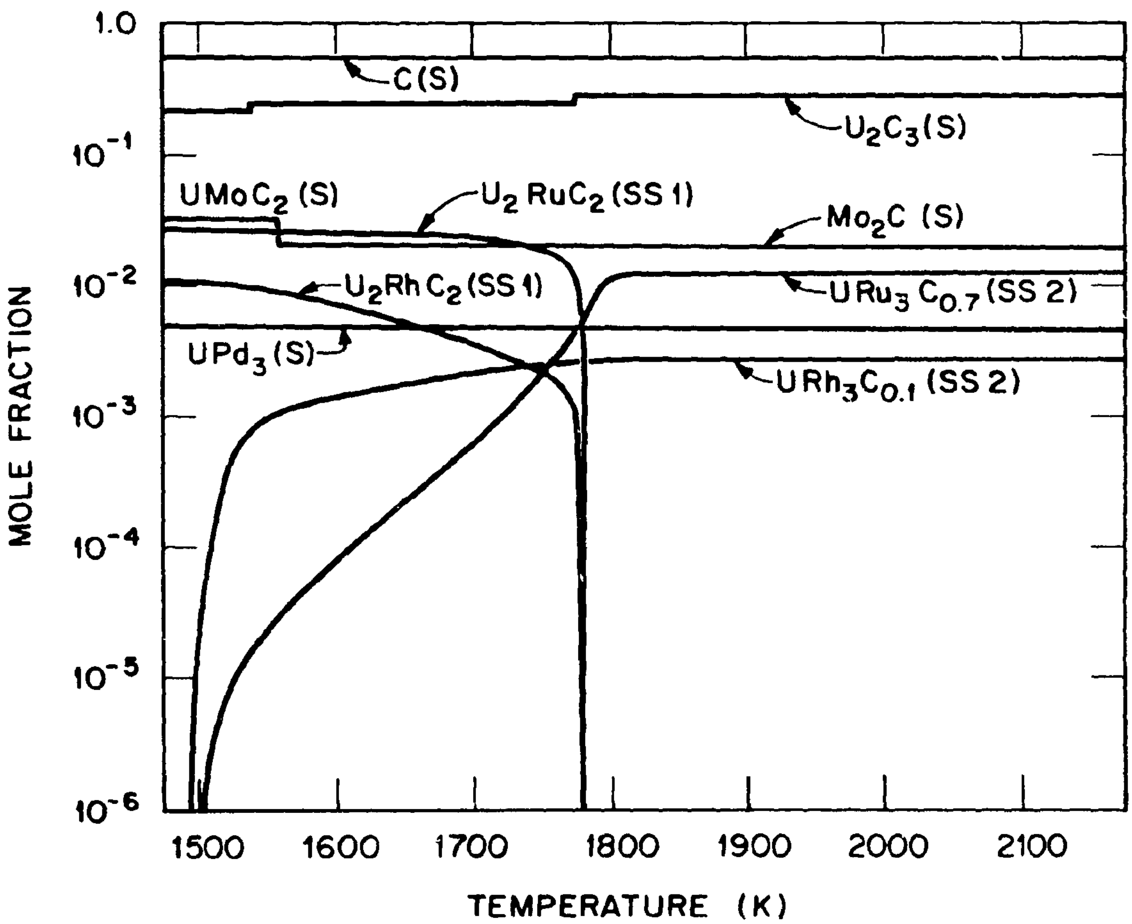

Fig. 18. Mole fraction of phases formed in MEU UC_2 fuel irradiated to 25% FIMA versus temperature. Calculated atom ratios based on 100 initial U atoms (see Table A.2) were: C = 300, U = 75, Mo = 5.88, Ru = 3.42, Rh = 1.09, Pd = 1.87.

4.3 Proposed Mode of SiC—Fission Product Interaction

In Sects. 3.2.2 and 3.3.3, we reported that uranium as UO_2 and molybdenum in UC_2 remain in place in the various kernels even at high temperatures. Apparently their vapor pressures (see Fig. 1) and diffusion rates are too small to effectively transfer them. Uranium as UC_2, and the noble metals, either as elements or compounds, have high enough vapor pressures to transfer some or all of the gaseous metal atoms from the kernels into the buffer layers. All of the metals are then able to diffuse through the inner pyrolytic carbon layers and concentrate along portions of the iLTI and SiC interface (see Fig. 12).

According to the Pd-Si-C phase diagram,[32] recently reconfirmed,[33] palladium in contact with SiC can form Pd_3Si or Pd_2Si as seen in Fig. 19. Since there were no temperatures given with the diagram, we assume that it is valid up to the liquidus temperature. The following phases are in equilibrium in the indicated areas:

1. Pd_2Si, SiC, C;
2. Pd_2Si, Pd_3Si, C;
3. Pd, Pd_3Si, C.

The interaction between palladium and SiC may be pictured as follows: Pd-area 3-area 2-area 1-SiC. The Pd-Si phase diagram,[34] shown in Fig. 20, indicates that Pd_3Si melts incongruently at 960°C and Pd_2Si melts at 1330°C. Area 3, which is palladium rich, forms a low-melting eutectic at 760°C. The other two eutectics on the Pd-Si phase diagram involve excess silicon and PdSi, neither of which is expected.

The conclusion is that melting will occur on the palladium-rich side of the Pd-SiC interface as soon as interaction begins. This can be viewed as either fortunate or unfortunate. On the good side, if melting occurs in the SiC-rich end of the interface, the failure rate will probably be more severe. On the bad side, melting in the palladium-rich end probably accelerates material transport via the liquid phase. One other point should be noted on the Pd-Si phase diagram. If free silicon were in the deposited SiC, then melting caused by the silicon-rich eutectic

ORNL DWG 79-1587R

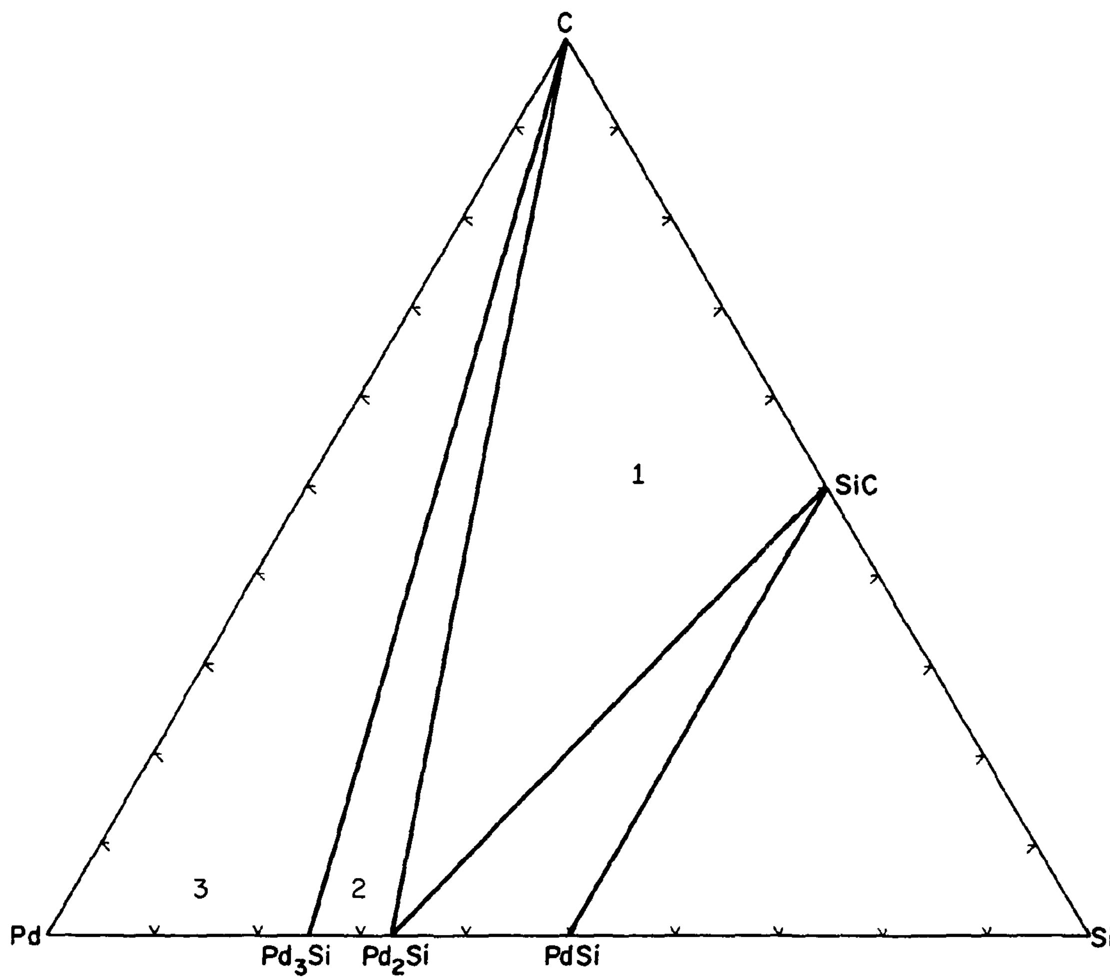

Fig. 19. Phase diagram of the Pd-Si-C system.

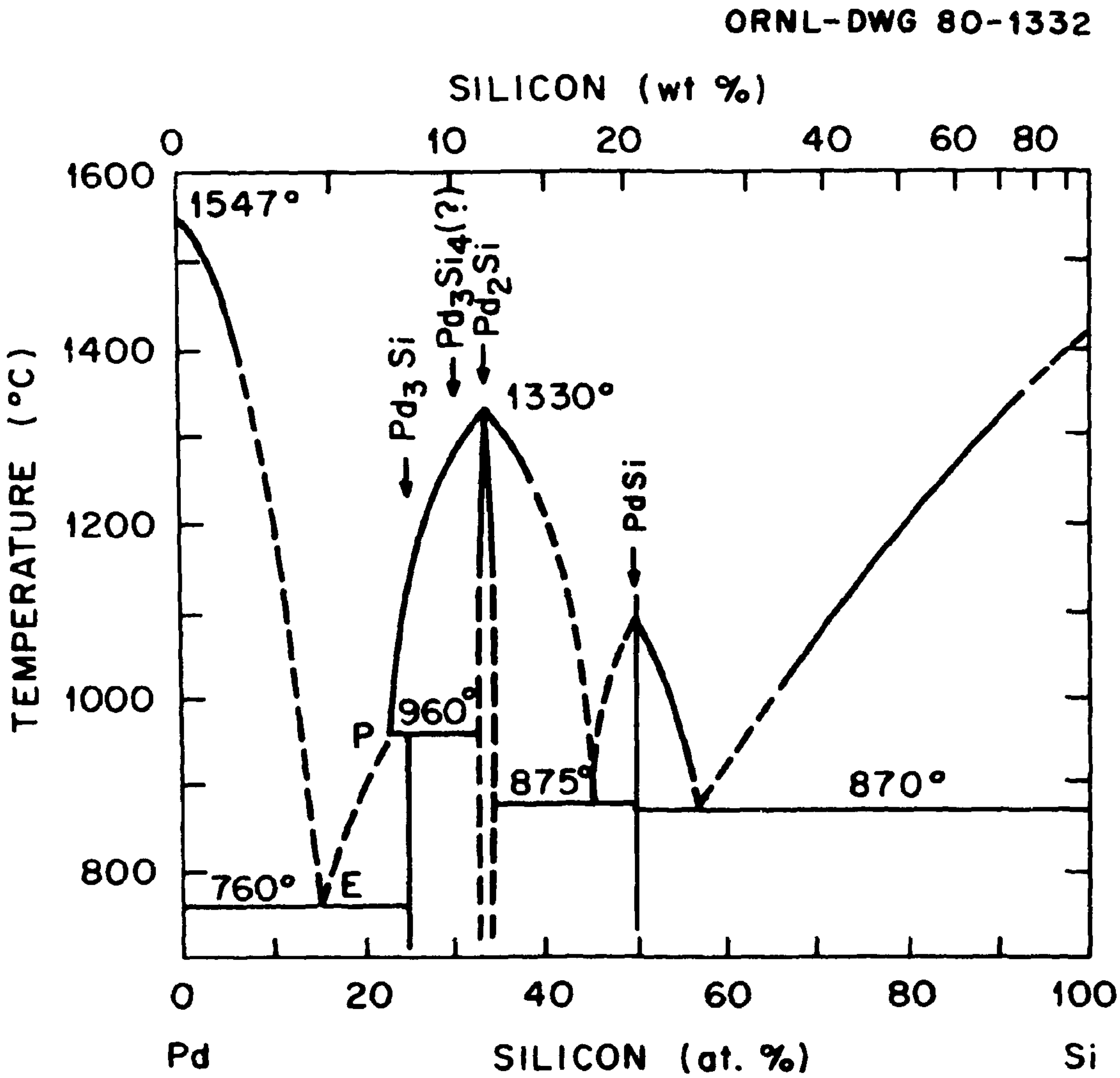

Fig. 20. Phase diagram of the Pd-Si system.

might occur in these areas. Current efforts to completely characterize various deposited SiC layers have not been able to detect free silicon.[35] It is speculated that if free silicon is there, it will be in very small quantities and will be found as a thin layer in the grain boundaries.

In Triso-coated UC_2 or UO_2/UC_2 particles containing palladium, both uranium and palladium have significant vapor pressures. Thermodynamic calculations indicate that the most stable palladium-containing compound in these particles is UPd_3 rather than the Pd-Si compounds calculated for the UO_2 system. Our experimental results seem to verify this. In Figs. 8, 9, 13, and 14, wherever palladium is found, uranium is found also, even in the SiC layer.

Possible compound formation in the U-Pd-Si-C system was also investigated. Compounds of the type MPd_2Si_2 and MRh_2Si_2, where M represents La, Ce, Pr, Nd, Sm, Eu, Gd, Tb, Dy, Ho, Er, and Y, have been reported.[37] These have the $ThCr_2Si_2$-type structure.[37] An arc-melted sample was prepared from the pure elements with the molar ratio U:Pd:Si:C of 1:2:2:2.67, and is shown in Fig. 21. If the U-Pd-Si-C compound were not stable, the arc-melted sample would have contained UC_2, UPd_3, and SiC in the ratio 0.33:0.67:2. However, the three phases in Fig. 21 appeared to be Pd-Si (black phase) and phases having U:Pd:Si ratios of 2:1:2 (white phase) and 1:3:3 (gray phase). These ratios were determined by quantitative analysis of each phase with the EMP and quantitative metallography. These compounds may also contain carbon, but this element cannot be detected with the EMP. Carbide formation is indicated, however, since no free carbon was detected metallographically, and no weight loss occurred during arc melting. One possible carbide composition would be $UPd_3Si_3C_6$. Further work is planned to characterize these compounds.

It is a curious and currently unexplainable fact that the thinning rates in the oxides vs either oxide-carbide or carbide systems are comparable. In the oxide system, the Pd-Si compounds should be formed. However, the break in the thinning rate (Fig. 17) at $\sim$1425°C is above the 1330°C melting temperature of Pd_2Si. Furthermore, the in-reactor data was for all three kernel types[9] and no difference in thinning rate

ORNL-PHOTO 5059-80

Fig. 21. An arc-melted specimen having the overall molar composition ratio of U:Pd:Si:C of 1:2:2:2.67. Three phases are present.

could be noted, but all of the data for the oxide systems was below the melting temperature of Pd_2Si. It is expected that the C + Pd_2Si + SiC solid equilibrium would have been present, with any unreacted Pd liquids reacting with SiC to form a possibly protective layer of Pd_2Si on the SiC interface. In the oxide-carbide or carbide systems, the melting of UPd_3 at ∿1640°C could be interpreted as causing the abrupt increase in the thinning rate data at that temperature (Fig. 17). Thus, it may be relevant to fit all the data below 1640°C, but this was not done here.

The UPd_3 in the SiC layer might explain why uranium was found in the SiC hulls in an irradiated HTGR fuel reprocessing study.[37] The SiC hulls of fuel elements irradiated in the Peach Bottom HTGR contained as much as 0.6 wt % uranium. However, this association of palladium and uranium has never been reported for irradiated LEU or MEU UC_2 fuel.

From the photomicrographs shown in Figs. 12(*a*) through 12(*j*), it appears possible to follow the fission product—SiC interaction sequence. First, fission products accumulated at the SiC-iLTI interface. The accumulation was not uniformly distributed. Pockets of fission products formed, and it was at these points that the SiC layer began to be attacked, as seen in Figs. 12(*a*) and 12(*b*). In Figs. 12(*c*) and 12(*d*), it looks as if the fission products have penetrated into the SiC layer about halfway; however, we learned from microprobe analysis that they had breached the SiC layer and entered into the oLTI layer. This same conclusion was reached in a previous paper.[10] (Complete penetration of the SiC layer is best detected by looking for darkened areas at the SiC-oLTI interface.) As more fission products passed through the SiC layer, they seeped along the SiC-oLTI interface and out into the oLTI layer. During this period, the SiC layer began to erode, as seen in Figs. 12(*e*) and 12(*f*). Further heat treatment [Figs. 12(*g*) through 12(*j*)] resulted in complete erosion of the SiC layer and complete penetration of the oLTI by fission products.

A Triso-coated $PuO_{1.81}$ particle, irradiated in the Peach Bottom Reactor to approximately 63% FIMA,[38] is shown in Fig. 22. The SiC layer has been breached, and fission products have completely penetrated the oLTI

ORNL-PHOTO Y167285

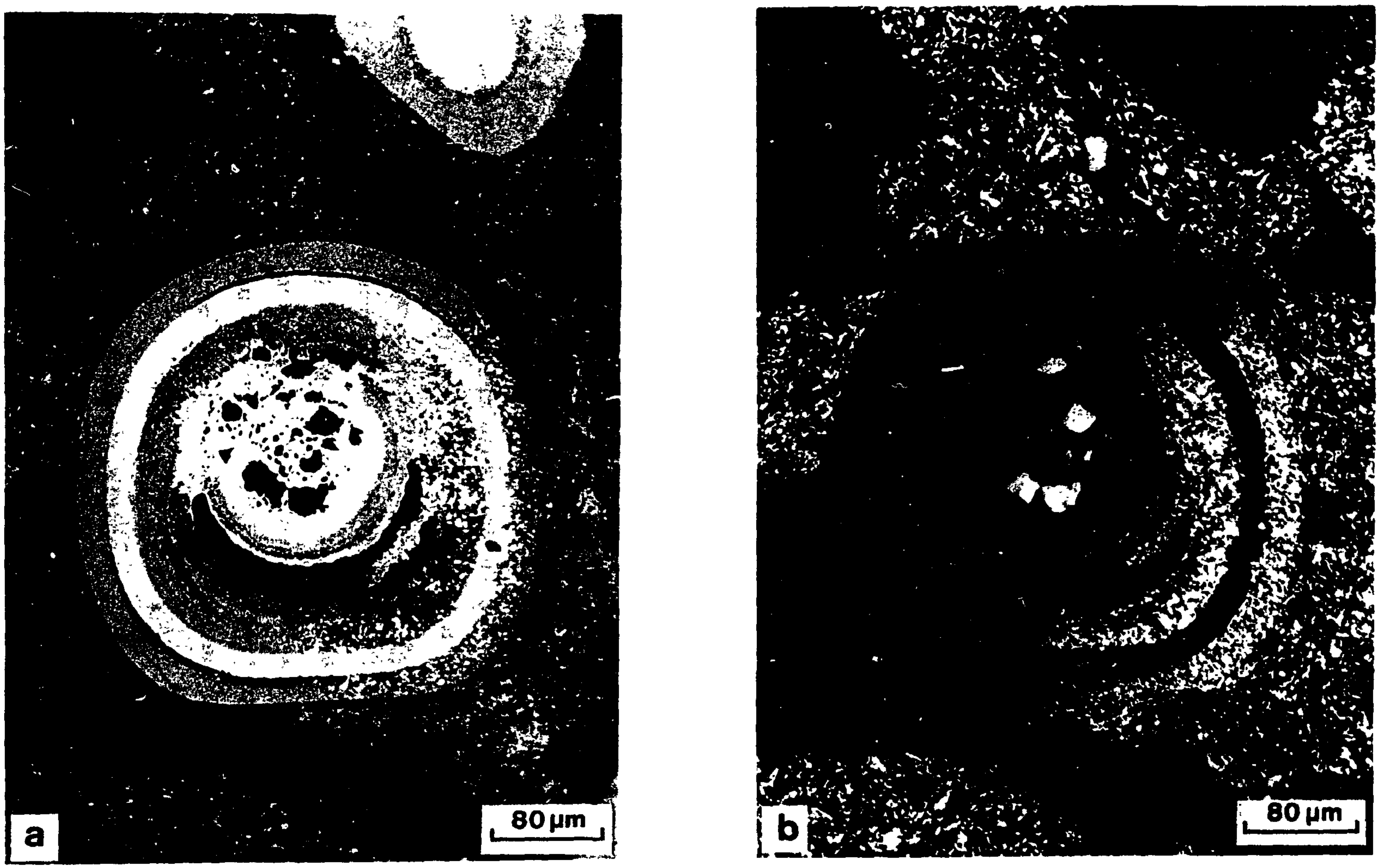

Fig. 22. Optical micrographs of Triso-coated $PuO_{1.81}$ particles irradiated to 63% FIMA. (*a*) Bright field; (*b*) polarized light.

layer. The photomicrographs of this irradiated Triso-coated particle look very much like those of the heat treated, simulated, Triso-coated UC_2 plus Mo-Ru-Pd-La particles displayed in Fig. 12.

5. CONCLUSIONS

1. After full burnup, the concentration of the fission products Mo, Ru, Rh, Pd, Ag, and Cd can be higher in MEU fuel than in HEU fuel, depending on the size ratio of the Triso-coated kernels.

2. Sound samples of simulated Triso-coated fuel particles containing varying amounts of the above elements were made, except for Triso-coated fuel particles containing cadmium.

3. Rhodium and palladium at concentrations found after full burnup will react with SiC in an MEU Triso-coated oxide or carbide fuel. Silver at a concentration 100 times that at full burnup reacts with SiC in an MEU Triso-coated oxide fuel.

4. Interactions of Rh-SiC and Pd-SiC can be measured by microprobe or optical microscopy, but not by radiography. As-deposited SiC is translucent when viewed under polarized or oblique light. Simulated fission-product interactions with SiC can be observed under the polished surface with a stereomicroscope. Interactions in irradiated particles cannot be seen by this technique because SiC becomes opaque during irradiation.

5. In Triso-coated UO_2, palladium interacts with the SiC, probably forming palladium silicides and palladium-rich eutectics that will melt at HTGR fuel operating temperatures. The palladium that interacts with the SiC in Triso-coated UC_2 or UO_2/UC_2 particles is always associated with uranium, possibly as UPd_3 or a U-Pd-Si-C compound.

6. Above 1673 K, the rate of SiC thinning due to fission product—SiC interaction occurs in the order palladium > rare earths > rhodium.

7. The rate of SiC thinning by palladium is not influenced by kernel composition under the conditions studied.

8. After the SiC layer is breached, the fission products enter the oLTI layer. They first seep along the SiC-oLTI interface and then diffuse completely through the oLTI.

ACKNOWLEDGMENTS

The authors wish to thank the following individuals for their contributions to this study: C. A. Culpepper of the Solid State Division, and C. S. Morgan, Jr., and R. Johnson of the Metals and Ceramics Division for helping to prepare the kernel compositions; J M Robbins, C. Hamby, Jr., and B. R. Chilcoat, all of the Metals and Ceramics Division, for Triso-coating the kernels; C. A. Culpepper, Solid State Division, and R. J. Lauf, R. S. Crouse, B. C. Leslie, N. W. Atchley, W. H. Warwick, and W. J. Mason of the Metals and Ceramics Division for their assistance in examining the particles. Rosemary Robertson, Betty Drake, and Amy Harkey helped prepare the manuscript for publication.

REFERENCES

1. C. L. Smith, "SiC-Fission Product Reactions in HTGR TRISO UC_2 and UC_xO_y Fissile Fuel. Part 1: Kinetics of Reactions in a Thermal Gradient," *J. Am. Ceram. Soc.* 62(11-12), 600-606 (1979).

2. H. Grübmeier, A. Naoumidis, and B. A. Thiele, "Silicon Carbide Corrosion in High-Temperature Gas-Cooled Reactor Fuel Particles," *Nucl. Technol.* 35, 413 (1977).

3. F. J. Homan et al., "Stoichiometric Effects on Performance of High-Temperature Gas-Cooled Reactor Fuels from the U-C-O System," *Nucl. Technol.* 35, 428 (1977).

4. T. N. Tiegs, T. B. Lindemer, and T. J. Henson, "Fission Product Behavior in UC_xO_y Fissile Particles Made from Weak-Acid-Resins," submitted for publication in *Nuclear Technology*.

5. P. E. Brown et al., *Metal Fission Product Behaviour in HTR UO_2-Coated Particle Fuel*, AERE-R8065 (June 1975).

6. F. J. Homan et al., *Irradiated Performance of HTGR Fuel Rods in HFIR Experiments HRB-4 and -5,* ORNL-5115 (June 1976).

7. T. N. Tiegs et al., *Irradiated Performance of HTGR Fuel in HFIR Capsule 31,* ORNL-5510 (May 1979).

8. T. N. Tiegs and J M Robbins, *Irradiation Performance of HTGR Fuel in HFIR Capsule 33,* ORNL-5539 (June 1979).

9. T. N. Tiegs, *Fission Product Palladium-SiC Interaction in Coated Particle Fuels*, ORNL/TM-7203 (April 1980).

10. R. L. Pearson and T. B. Lindemer, "The Interaction of LaC_2 and NdC_2 with SiC in HTGR Particles," p. 357 in vol. 3 of *Proceedings of ANS Thermal Reactor Safety Meeting*, June 31-Aug. 4, 1977, Sun Valley, Idaho.

11. R. L. Pearson and T. B. Lindemer, *Simulated Fission Product Oxide Behavior in Triso-Coated HTGR Fuel,* ORNL/TM-6741 (August 1979).

12. D. R. Olander, *Fundamental Aspects of Nuclear Reactor Fuel Elements*, TID-26711-P1 (1976), pp. 172-98.

13. H. Huschka and P. Vygen, "Coated Fuel Particles: Requirements and Status of Fabrication Technology," *Nucl. Technol.* 35, 238 (1977).

14. T. B. Lindemer and H. J. de Nordwall, *An Analysis of Chemical Failure of Coated UO_2 and Other Oxide Fuels in the High-Temperature Gas-Cooled Reactor*, ORNL-4926 (January 1974).

15. D. E. LaValle, D. A. Costanzo, W. J. Lackey, and A. P. Cuputo, "The Determination of Defective Particle Fraction in High Temperature Gas-Cooled Reactor Fuels," *Nucl. Technol.* 33, 290 (1977).

16. J. I. Federer, *Fluidized Bed Deposition and Evaluation of Silicon and Microspheres,* ORNL/TM-5152 (January 1977).

17. T. B. Lindemer and R. L. Pearson, "Kernel Migration for HTGR Fuels from the System Th-U-Pu-C-O-N," *J. Am. Ceram. Soc.* 60(1-2), 5-14 (1977).

18. General Atomic Company, *Fort St. Vrain MEU Program Final Report,* GA-A15216 (July 1979), p. 20.

19. H. Holleck, "Ternary Phase Equilibria in the Systems Actinide-Transition Metal-Carbon and Actinide-Transition Metal-Nitrogen," p. 213 in vol. 2 of *Proceedings of IAEA Thermodynamics of Nuclear Materials Meeting*, Oct. 21-25, 1974, Vienna, Austria.

20. T. M. Besmann, *SOLGASMIX-PV, A Computer Program to Calculate Equilibrium Relationships in Complex Chemical Systems*, ORNL/TM-5775 (April 1977).

21. M. Tetenbaum, A. Sheth, and W. Olson, *A Review of the Thermodynamics of the U-C, Pu-C, and U-Pu,C Systems*, ANL-AFP-8 (June 1975).

22. R. Hultgren et al., *Selected Values of the Thermodynamic Properties of the Elements*, American Society for Metals, Metals Park, Ohio, 1973.

23. O. Kubaschewski and C. B. Alcock, *Metallurgical Thermochemistry*, Pergamon Press, New York, 1979.

24. M. G. Naraine and H. B. Bell, "Free Energy of Formation of $UMoC_2$ and Phase Behaviour in the U-Mo-C System," *J. Nucl. Mater.* 49, 329-32 (1973/74).

25. N. Lorenzelli, *Etude Metallurgique et Thermodynamique d'uns Combustible Carbure Contenant des Produits de Fission Inactifs: une "Simulation" de Combustible Nucleaire Irradie*, Ph.D. Thesis, University of Paris, France, April 1973.

26. Dow Chemical Company, Thermal Research Laboratory, *JANAF Thermochemical Tables*, 2nd ed., NSRDS-NBS 37, National Bureau of Standards, Washington, D.C., 1971.

27. T. G. Chart, *A Critical Assessment of Thermochemical Data for Transition Metal-Silicon Systems*, NPL Report Chem. 18 (August 1972).

28. M. G. Naraine and H. B. Bell, "Thermodynamic and Phase Behaviour in the U-Rh-C System," *J. Nucl. Mater.* 50, 83-90 (1974).

29. E. Smailos, *Reaction Behavior of Fission Products in Carbide and Nitride Fuel Based on Simulation Investigations*, EURFNR-1179 (March 1974).

30. H. Holleck and H. Kleykamp, "Phasengleichgewichte und Thermodynamische Untersuchungen im System Uran-Rhodium-Kohlenstoff," *J. Nucl. Mater.* 45, 47-54 (1972/73).

31. H. Holleck and H. Kleykamp, "Zur Konstitution und Thermodynamik im System Uran-Ruthenium-Kohlenstoff," *J. Nucl. Mater.* 35, 158-66 (1970).

32. A. Searcy and L. Finnie, "Stability of Solid Phases in the Ternary Systems of Silicon and Carbon with Rhenium and the Six Platinum Metals," *J. Am. Ceram. Soc.* 45(6), 268-73 (1962).

33. H. Suzaki et al., "Reactions Between SiC and Pd or CeO_2 at High Temperatures," *J. Nucl. Sci. Technol.* 14(6), 44-48 (June 1977).

34. R. P. Elliott, *Constitution of Binary Alloys, First Supplement,* McGraw Hill, New York, 1965, p. 732.

35. R. J. Lauf, ORNL, personal communication with R. L. Pearson (November 1979).

36. R. Ballestracci, *C. R. Acad. Sci. Ser. B* 282(13), 291-92 (1976).

37. K. H. Lin and W. E. Clark, *High-Level Solid Wastes from HTGR Fuel Reprocessing*, GCR-77/10 (August 1977).

38. T. N. Tiegs, "Irradiation Performance of Pu-Containing Coated-Particle Fuels," *Trans. Am. Nucl. Soc.* 28, 175 (1978).

39. B. F. Rider and M. E. Meek, *Compilation of Fission Product Yields,* NEDO-12154-2 (July 1977).

APPENDIXES

Appendix A. CALCULATION OF FISSION PRODUCT INVENTORIES IN HTGR FUELS

The proportion of the uranium and plutonium isotopes fissioning during irradiation is dependent on the initial uranium enrichment. Their accumulative fission yields are listed in Table A.1 and are plotted in Fig. A.1.[38] Each fission product listed consists of one or more isotopes and may include the daughters of radioactive precursors which have decayed during the lifetime of the HTGR elements. End-of-life fission product concentrations are calculated from the formulas:

$$\text{Conc} = \frac{\text{FP atoms}}{\text{Particle}} = \sum_{^{235}\text{U},\,^{239}\text{Pu},\,^{241}\text{Pu}} \left(\frac{\text{Atoms fissioned}}{\text{Particle}}\right)_i \left(\frac{\text{FP atoms}}{\text{Fission}}\right)_i$$

$$= \frac{\text{Initial HM atoms}}{\text{Particle}} \sum_{^{235}\text{U},\,^{239}\text{Pu},\,^{241}\text{Pu}} (\text{Yield})_i \cdot (\text{FIMA})_i \qquad (1)$$

$$\frac{(\text{Conc})_{\text{MEU}}}{(\text{Conc})_{\text{HEU}}} = \frac{D^3_{\text{MEU}} \sum_i Y_i F_i}{D^3_{\text{HEU}} \sum_i Y_i F_i} \; . \qquad (2)$$

A comparison of the relevant fission product inventories in several combinations of MEU and HEU fuels which have reached full burnup is found in Table A.2. From the MEU/HEU ratio column, it is clear that in this study of Triso-coated LEU or MEU fuels, we are particularly interested in the fission product palladium and perhaps in silver and cadmium, although their concentrations are quite low.

Table A.1. Accumulated fission product yields
(Based on 100 fissions at thermal neutron energy.)

Atomic No.	Fission product	Percent yield			
		^{233}U	^{235}U	^{235}Pu	^{241}Pu
32	Ge	0.020	0.005	0.004	0.001
33	As	0.008	0.001	0.001	0.000
34	Se	1.028	0.530	0.402	0.172
35	Br	0.291	0.196	0.175	0.062
36	Kr	6.073	3.791	1.658	1.334
37	Rb	5.711	3.566	1.433	1.110
38	Sr	12.378	9.565	3.481	2.627
39	Y	6.287	4.877	1.699	1.177
40	Zr	32.612	31.040	18.876	15.743
41	Nb	0.000	0.000	0.000	0.000
42	Mo	21.231	24.416	22.950	20.204
43	Tc	4.891	6.104	6.169	6.303
44	Ru	6.716	11.138	17.954	19.162
45	Rh	1.675	3.040	6.951	6.133
46	Pd	0.947	1.609	15.905	22.561
47	Ag	0.045	0.033	1.654	2.249
48	Cd	0.074	0.067	0.575	1.052
49	In	0.012	0.010	0.036	0.040
50	Sn	0.319	0.130	0.436	0.225
51	Sb	0.144	0.058	0.195	0.091
52	Te	2.802	2.119	3.105	2.007
53	I	2.140	0.827	2.001	0.985
54	Xe	28.386	27.810	30.983	28.014
55	Cs	12.811	12.930	13.661	13.398
56	Ba	6.008	6.770	6.144	6.859
57	La	6.311	6.385	5.681	5.881
58	Ce	13.114	12.183	10.566	11.385
59	Pr	6.536	5.838	5.289	5.028
60	Nd	18.182	20.640	16.217	18.781
61	Pm	1.710	2.229	2.050	2.392
62	Sm	1.327	1.833	2.883	3.671
63	Eu	0.125	0.193	0.535	0.800
64	Gd	0.019	0.022	0.245	0.423
65	Tb	0.001	0.001	0.021	0.049
Total rare earths		47.325	49.324	43.487	48.410

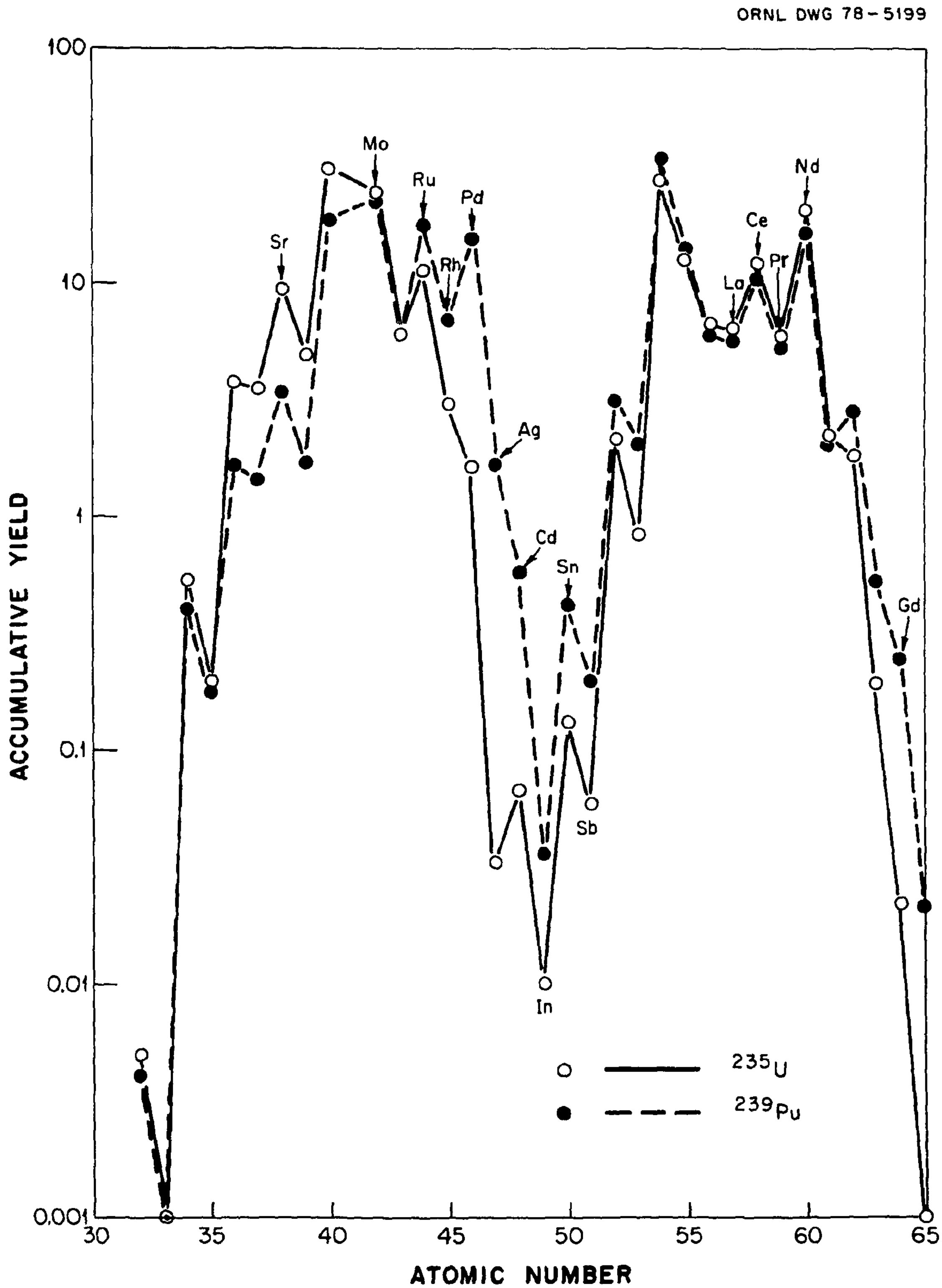

Fig. A.1. Accumulative fission product yields for ^{235}U and ^{239}Pu.

Table A.2. Comparison of relevant fission product inventory (Based on 100 initial U atoms.)

Fission product	MEU fuel[a] (atoms)	HEU fuel[b] (atoms)	MEU/HEU ratio Case 1[c]	Case 2[d]	Case 3[e]
Mo	5.88	17.53	0.335	1.13	1.80
Ru	3.42	8.12	0.422	1.42	2.26
Rh	1.09	2.24	0.487	1.64	2.61
Pd	1.87	1.40	1.34	4.52	7.18
Ag	0.166	0.050	3.32	11.20	17.79
Cd	0.075	0.058	1.29	4.35	6.91
Rare earths	11.87	35.41	0.335	1.13	1.80

[a] ∿25% FIMA (^{235}U = 15.80%; ^{239}Pu = 6.63%; ^{241}Pu = 2.48%).

[b] ∿72% FIMA (^{235}U = 70.42%; ^{239}Pu = 1.15%; ^{241}Pu = 0.36%).

[c] MEU particle diam = 200 μm; HEU particle diam = 200 μm.

[d] MEU particle diam = 300 μm; HEU particle diam = 200 μm.

[e] MEU particle diam = 350 μm; HEU particle diam = 200 μm.

Appendix B. DETERMINATION OF APPROXIMATE KERNEL COMPOSITIONS LISTED IN TABLE 1

B.1 Calculations for Set 1

<u>Sample 1-1 (Mo-Ru-Rh-Pd)</u>

[Assume 20% ^{235}U enrichment and 20% FIMA (16% ^{235}U; 4% ^{239}Pu)]

$(conc)_{Mo}$ = (0.16)(24.42) + (0.04)(22.95) = 4.83 atoms/100 initial U atoms;
$(conc)_{Ru}$ = (0.16)(11.14) + (0.04)(17.95) = 2.50 atoms/100 initial U atoms;
$(conc)_{Rh}$ = (0.16)(3.04) + (0.04)(6.95) = 0.77 atoms/100 initial U atoms;
$(conc)_{Pd}$ = (0.16)(1.61) + (0.04)(15.91) = 0.90 atoms/100 initial U atoms;

In weight percent:

Mo =	4.83 x 95.94 =	463.39	=	52.0%
Ru =	2.50 x 101.07 =	252.68	=	28.4%
Rh =	0.77 x 102.91 =	79.24	=	8.9%
Pd =	0.90 x 106.40 =	95.76	=	10.7%
		891.07		

<u>Sample 1-2 (UC_2 plus Mo-Ru-Rh-Pd)*</u>

[Assume 93% ^{235}U enrichment and 64% FIMA (64% ^{235}U)]

$(conc)_{Mo}$ = (0.64)(24.42) = 15.62 atoms/100 initial U atoms;
$(conc)_{Ru}$ = (0.64)(11.14) = 7.13 atoms/100 initial U atoms;
$(conc)_{Rh}$ = (0.64)(3.04) = 1.95 atoms/100 initial U atoms;
$(conc)_{Pd}$ = (0.64)(1.61) = 1.03 atoms/100 initial U atoms;
$(conc)_{U}$ = 100 - 64 = 36;
$(conc)_{C}$ = 85.

---

*The calculations performed for this sample indicated that a fully burned-up HEU fuel contained more Pd than did a fully burned-up MEU fuel. This is in error because early in this study we used the wrong proportion of fissioning isotopes. Fortuitously, the Pd in a correctly calculated HEU fuel is very close to the amount added to sample 1-2. Assuming 20% U enrichment and 25% FIMA (15.8% ^{235}U; 6.63% ^{239}Pu; 2.48% ^{241}Pu), the correct mixture for this sample should have been Mo = 2.63 wt %; Ru = 1.61 wt %; Rh = 0.52 wt %; Pd = 0.93 wt %; U = 83.13 wt %; and C = 11.18 wt %.

In weight percent:

Mo	=	15.62	x	95.94	=	1,499	=	12.37%
Ru	=	7.13	x	101.07	=	721	=	5.95%
Rh	=	1.95	x	102.91	=	201	=	1.66%
Pd	=	1.03	x	106.40	=	110	=	0.91%
U	=	36.00	x	238.04	=	8,569	=	70.70%
C	=	85.00	x	12.01	=	1,021	=	8.42%
						12,121		

<u>Sample 1-3 (UO_2 plus Ag)</u>

[Assume 20% U enrichment and 20% FIMA (16% ^{235}U; 4% ^{239}Pu)]

$(conc)_{Ag}$ = (0.16)(0.033) + (0.04)(1.65) = 0.071 atoms/100 initial U atoms;
$(conc)_U$ = 100 - 20 = 80.

In weight percent:

Ag	=	0.071	x	107.87	=	7.7	=	0.068%
UO_2	=	80.0	x	270.04	=	21,603.0	=	99.964%
						21,610.7		

This amount of Ag is too small to detect by dispersive x rays. To be sure we can detect it, we will add 100 times as much Ag.

Ag	=	770	=	3.4%
UO_2	=	21,603	=	96.6%
		22,373		

B.2 Calculations for Set 2

<u>Sample 2-1 (UC_2 plus Mo-Ru-Pd)</u>

[Assume 20% ^{235}U enrichment and 25% FIMA (13.75% ^{235}U; 11.25% ^{239}Pu)]

$(conc)_{Mo}$ = (0.1375)(24.42) + (0.1125)(22.95) = 5.94 atoms/100 initial U atoms;
$(conc)_{Ru}$ = (0.1375)(11.14) + (0.1125)(17.95) = 3.55 atoms/100 initial U atoms;
$(conc)_{Rh}$ = (0.1375)(3.04) + (0.1125)(6.95) = 1.20 atoms/100 initial U atoms;
$(conc)_{Pd}$ = (0.1375)(1.61) + (0.1125)(15.91) = 2.01 atoms/100 initial U atoms;
$(conc)_U$ = 100 - 25 = 75;
$(conc)_C$ = 200.

In order to overcome the Rh-Pd identity problem, the atoms of Rh will be substituted by Ru since they behave alike chemically. We also will increase the amount of Mo, Ru, and Pd added to the UC_2 by a factor of 4 in order to assure ourselves that we will be able to detect them by dispersive x rays. The addition of these extra quantities of the fission products is permissible only if no new phases are formed within the particles. Calculations using the computer program SOLGASMIX-PV[20] were made, assuring ourselves that no new phases would be introduced.

In weight percent:

$$
\begin{aligned}
Mo &= (5.94 \times 4) \times 95.94 = 2{,}280 = 9.01\% \\
Ru &= (4.75 \times 4) \times 101.07 = 1{,}920 = 7.58\% \\
Pd &= (2.01 \times 4) \times 106.91 = 860 = 3.40\% \\
U &= 75.0 \times 238.04 = 17{,}853 = 70.52\% \\
C &= 200.0 \times 12.01 = \underline{2{,}402} = 9.49\% \\
& \qquad 25{,}315
\end{aligned}
$$

<u>Sample 2-2 (UC_2 plus Mo-Ru-Rh)</u>

[Assume 20% ^{235}U enrichment and 25% FIMA (13.75% ^{235}U; 11.25% ^{239}Pu)]

$(conc)_{Mo}$ = 5.94 atoms/100 initial U atoms (see sample 2-1);
$(conc)_{Ru}$ = 3.55 atoms/100 initial U atoms (see sample 2-1);
$(conc)_{Rh}$ = 1.20 atoms/100 initial U atoms (see sample 2-1);
$(conc)_{U}$ = 100 - 25 = 75;
$(conc)_{C}$ = 200.

No Pd was added to the sample in order to avoid the Rh-Pd identification problem, and the amount of Mo, Ru, and Rh added to the UC_2 was increased by a factor of 4 to assure ourselves that we would be able to detect them by dispersive x rays. No new phases were introduced.

In weight percent:

$$
\begin{aligned}
Mo &= (5.94 \times 4) \times 95.94 = 2{,}280 = 9.32\% \\
Ru &= (3.55 \times 4) \times 101.07 = 1{,}436 = 5.87\% \\
Rh &= (1.20 \times 4) \times 102.91 = 492 = 2.01\% \\
U &= 75.0 \times 238.04 = 17{,}853 = 72.98\% \\
C &= 200.0 \times 12.01 = \underline{2{,}402} = 9.82\% \\
& \qquad 24{,}463
\end{aligned}
$$

Sample 2-3 (UC_2 plus Mo-Ru-Pd-La)

[Assume 20% ^{235}U enrichment and 25% FIMA (13.75% U; 11.25% ^{239}Pu)]

$(conc)_{Mo}$ = 5.94 atoms/100 initial U atoms (see sample 2-1);

$(conc)_{Ru}$ = 4.75 atoms/100 initial U atoms (see sample 2-1);

$(conc)_{Pd}$ = 2.01 atoms/100 initial U atoms (see sample 2-1);

$(conc)_{R.E.}$* = (0.1375)(49.32) + (0.1125)(43.49) = 11.67 atoms/100 initial U atoms;

$(conc)_U$ = 100 - 25 = 75;

$(conc)_C$ = 200.

All of the rare earths will be added as La since they all behave alike chemically. The amount of Mo, Ru, and Pd added to the UC_2 was increased by a factor of 4 in order to assure ourselves that we would be able to detect them by dispersive x rays. No new phases were introduced.

In weight percent:

Mo =	(5.94 x 4)	x 95.94	= 2,280	=	8.46%
Ru =	(4.75 x 4)	x 101.07	= 1,920	=	7.13%
Pd =	(2.01 x 4)	x 106.91	= 860	=	3.19%
La =	(11.67)	x (138.91)	= 1,621	=	6.02%
U =	(75.0)	x (238.04)	= 17,853	=	66.28%
C =	(200.0)	x (12.01)	= 2,402	=	8.92%
			23,141		

Sample 2-4 (UO_2 plus Mo-Ru-Pd)

[Assume 20% ^{235}U enrichment and 25% FIMA (13.75% ^{235}U; 11.25% ^{239}Pu)]

$(conc)_{Mo}$ = 5.94 atoms/100 initial U atoms (see sample 2-1);

$(conc)_{Ru}$ = 4.75 atoms/100 initial U atoms (see sample 2-1);

$(conc)_{Pd}$ = 2.01 atoms/100 initial U atoms (see sample 2-1);

$(conc)_U$ = 100 - 25 = 75.

The amount of Mo, Rh, and Pd added to the UO_2 was increased by a factor of 4 in order to assure ourselves that we would be able to detect them by dispersive x rays. No new phases were introduced.

*R.E. = rare earths.

In weight percent:

Mo =	(5.94 x 4) x 95.94 =	2,230 =	9.00%
Ru =	(4.75 x 4) x 101.07 =	1,932 =	7.63%
Pd =	(2.01 x 4) x 106.91 =	860 =	3.40%
UO_2 =	(75.0) x 270.04 =	20,253 =	79.97%
		25,325	

Sample 2-5 (UO_2 plus Mo-Ru-Rh)

[Assume 20% ^{235}U enrichment and 25% FIMA (13.75% ^{235}U; 11.25% ^{239}Pu)]

$(conc)_{Mo}$ = 5.94 atoms/100 initial U atoms (see sample 2-1);

$(conc)_{Ru}$ = 3.55 atoms/100 initial U atoms (see sample 2-1);

$(conc)_{Rh}$ = 1.20 atoms/100 initial U atoms (see sample 2-1);

$(conc)_{U}$ = 100 - 25 = 75.

No Pd was added to the sample in order to avoid the Rh-Pd identification problem, and the amount of Mo, Ru, and Rh added to the UO_2 was increased by a factor of 4 in order to assure ourselves that we would be able to detect them by dispersive x rays. No new phases were introduced.

In weight percent:

Mo =	(5.94 x 4) x 95.94 =	2,280 =	9.32%
Ru =	(3.55 x 4) x 101.07 =	1,436 =	5.87%
Rh =	(1.20 x 4) x 102.91 =	492 =	2.01%
UO_2 =	(75.0) x 270.04 =	20,253 =	82.80%
		24,461	

Sample 2-6 (90% UO_2/10% UC_2 plus Mo-Ru-Pd)

[Assume 20% ^{235}U enrichment and 25% FIMA (13.75% ^{235}U; 11.25% ^{239}Pu)]

$(conc)_{Mo}$ = 5.94 atoms/100 initial U atoms (see sample 2-1);

$(conc)_{Ru}$ = 4.75 atoms/100 initial U atoms (see sample 2-1);

$(conc)_{Pd}$ = 2.01 atoms/100 initial U atoms (see sample 2-1);

$(conc)_{U}$ = 100 - 25 = 75.

The amount of Mo, Ru, and Pd added to the 90% UO_2/10% UC_2 mix was increased by a factor of 2.5 in order to assure ourselves that we would be able to detect them by dispersive x rays. No new phases were introduced at this level. Above factors of 2.5, another phase begins to appear.

In weight percent:

$$
\begin{aligned}
Mo &= (5.94 \times 2.5) \times 95.94 &&= 1{,}425 = 6.10\% \\
Ru &= (4.75 \times 2.5) \times 101.07 &&= 1{,}207 = 5.17\% \\
Pd &= (2.01 \times 2.5) \times 106.91 &&= 538 = 2.30\% \\
UO_2 &= (75.0) \times (270.04) \times 0.90 &&= 18{,}227 = 78.07\% \\
UC_2 &= (75.0) \times (260.06) \times 0.10 &&= \underline{1{,}950} = 8.35\% \\
& &&\quad 23{,}347
\end{aligned}
$$

Sample 2-7 (65% UO_2/35% UC_2 plus Mo-Ru-Pd)

[Assume 20% ^{235}U enrichment and 25% FIMA (13.75% ^{235}U; 11.25% ^{239}Pu)]

$(conc)_{Mo}$ = 5.94 atoms/100 initial U atoms (see sample 2-1);
$(conc)_{Ru}$ = 4.75 atoms/100 initial U atoms (see sample 2-1);
$(conc)_{Pd}$ = 2.01 atoms/100 initial U atoms (see sample 2-1);
$(conc)_{U}$ = 100 - 25 = 75.

The amount of Mo, Ru, and Pd added to the 65% UO_2/35% UC_2 mix was increased by a factor of 2.5 in order to assure ourselves that we would be able to detect them by dispersive x rays. No new phases were introduced. Above factors of 2.5, another phase begins to appear.

In weight percent:

$$
\begin{aligned}
Mo &= (5.94 \times 2.5) \times 95.94 &&= 1{,}425 = 6.15\% \\
Ru &= (4.75 \times 2.5) \times 101.07 &&= 1{,}207 = 5.21\% \\
Pd &= (2.01 \times 2.5) \times 106.91 &&= 538 = 2.32\% \\
UO_2 &= (75.0) \times (270.04) \times 0.65 &&= 13{,}164 = 56.84\% \\
UC_2 &= (75.0) \times (260.06) \times 0.35 &&= \underline{6{,}827} = 29.48\% \\
& &&\quad 23{,}161
\end{aligned}
$$

Sample 2-8 (UO_2 plus Ag)

[Assume 20% ^{235}U enrichment and 25% FIMA (13.75% ^{235}U; 11.25% ^{239}Pu)]

$(conc)_{Ag}$ = (0.1375 x 0.033) + (0.1125 x 1.65) = 0.190 atoms/100 initial U atoms;

$(conc)_{U}$ = 100 - 25 = 75.

In order to overcome the Rh-Pd identity problem, the atoms of Rh will be substituted by Ru since they behave alike chemically. We also will increase the amount of Mo, Ru, and Pd added to the UC_2 by a factor of 4 in order to assure ourselves that we will be able to detect them by dispersive x rays. The addition of these extra quantities of the fission products is permissible only if no new phases are formed within the particles. Calculations using the computer program SOLGASMIX-PV[20] were made, assuring ourselves that no new phases would be introduced.

In weight percent:

Mo	=	(5.94 x 4) x 95.94	=	2,280	=	9.01%
Ru	=	(4.75 x 4) x 101.07	=	1,920	=	7.58%
Pd	=	(2.01 x 4) x 106.91	=	860	=	3.40%
U	=	75.0 x 238.04	=	17,853	=	70.52%
C	=	200.0 x 12.01	=	2,402	=	9.49%
				25,315		

Sample 2-2 (UC_2 plus Mo-Ru-Rh)

[Assume 20% ^{235}U enrichment and 25% FIMA (13.75% ^{235}U; 11.25% ^{239}Pu)]

$(conc)_{Mo}$ = 5.94 atoms/100 initial U atoms (see sample 2-1);

$(conc)_{Ru}$ = 3.55 atoms/100 initial U atoms (see sample 2-1);

$(conc)_{Rh}$ = 1.20 atoms/100 initial U atoms (see sample 2-1);

$(conc)_{U}$ = 100 - 25 = 75;

$(conc)_{C}$ = 200.

No Pd was added to the sample in order to avoid the Rh-Pd identification problem, and the amount of Mo, Ru, and Rh added to the UC_2 was increased by a factor of 4 to assure ourselves that we would be able to detect them by dispersive x rays. No new phases were introduced.

In weight percent:

Mo	=	(5.94 x 4) x 95.94	=	2,280	=	9.32%
Ru	=	(3.55 x 4) x 101.07	=	1,436	=	5.87%
Rh	=	(1.20 x 4) x 102.91	=	492	=	2.01%
U	=	75.0 x 238.04	=	17,853	=	72.98%
C	=	200.0 x 12.01	=	2,402	=	9.82%
				24,463		

Sample 2-3 (UC_2 plus Mo-Ru-Pd-La)

[Assume 20% ^{235}U enrichment and 25% FIMA (13.75% U; 11.25% ^{239}Pu)]

$(conc)_{Mo}$ = 5.94 atoms/100 initial U atoms (see sample 2-1);

$(conc)_{Ru}$ = 4.75 atoms/100 initial U atoms (see sample 2-1);

$(conc)_{Pd}$ = 2.01 atoms/100 initial U atoms (see sample 2-1);

$(conc)_{R.E.}$* = (0.1375)(49.32) + (0.1125)(43.49) = 11.67 atoms/100 initial U atoms;

$(conc)_{U}$ = 100 - 25 = 75;

$(conc)_{C}$ = 200.

All of the rare earths will be added as La since they all behave alike chemically. The amount of Mo, Ru, and Pd added to the UC_2 was increased by a factor of 4 in order to assure ourselves that we would be able to detect them by dispersive x rays. No new phases were introduced.

In weight percent:

Mo =	(5.94 x 4) x 95.94	= 2,280	=	8.46%
Ru =	(4.75 x 4) x 101.07	= 1,920	=	7.13%
Pd =	(2.01 x 4) x 106.91	= 860	=	3.19%
La =	(11.67) x (138.91)	= 1,621	=	6.02%
U =	(75.0) x (238.04)	= 17,853	=	66.28%
C =	(200.0) x (12.01)	= 2,402	=	8.92%
		23,141		

Sample 2-4 (UO_2 plus Mo-Ru-Pd)

[Assume 20% ^{235}U enrichment and 25% FIMA (13.75% ^{235}U; 11.25% ^{239}Pu)]

$(conc)_{Mo}$ = 5.94 atoms/100 initial U atoms (see sample 2-1);

$(conc)_{Ru}$ = 4.75 atoms/100 initial U atoms (see sample 2-1);

$(conc)_{Pd}$ = 2.01 atoms/100 initial U atoms (see sample 2-1);

$(conc)_{U}$ = 100 - 25 = 75.

The amount of Mo, Rh, and Pd added to the UO_2 was increased by a factor of 4 in order to assure ourselves that we would be able to detect them by dispersive x rays. No new phases were introduced.

*R.E. = rare earths.

In weight percent:

Mo	=	(5.94 x 4) x 95.94	=	2,230	=	9.00%
Ru	=	(4.75 x 4) x 101.07	=	1,932	=	7.63%
Pd	=	(2.01 x 4) x 106.91	=	860	=	3.40%
UO_2	=	(75.0) x 270.04	=	20,253	=	79.97%
				25,325		

Sample 2-5 (UO_2 plus Mo-Ru-Rh)

[Assume 20% ^{235}U enrichment and 25% FIMA (13.75% ^{235}U; 11.25% ^{239}Pu)]

$(conc)_{Mo}$ = 5.94 atoms/100 initial U atoms (see sample 2-1);
$(conc)_{Ru}$ = 3.55 atoms/100 initial U atoms (see sample 2-1);
$(conc)_{Rh}$ = 1.20 atoms/100 initial U atoms (see sample 2-1);
$(conc)_{U}$ = 100 - 25 = 75.

No Pd was added to the sample in order to avoid the Rh-Pd identification problem, and the amount of Mo, Ru, and Rh added to the UO_2 was increased by a factor of 4 in order to assure ourselves that we would be able to detect them by dispersive x rays. No new phases were introduced.

In weight percent:

Mo	=	(5.94 x 4) x 95.94	=	2,280	=	9.32%
Ru	=	(3.55 x 4) x 101.07	=	1,436	=	5.87%
Rh	=	(1.20 x 4) x 102.91	=	492	=	2.01%
UO_2	=	(75.0) x 270.04	=	20,253	=	82.80%
				24,461		

Sample 2-6 (90% UO_2/10% UC_2 plus Mo-Ru-Pd)

[Assume 20% ^{235}U enrichment and 25% FIMA (13.75% ^{235}U; 11.25% ^{239}Pu)]

$(conc)_{Mo}$ = 5.94 atoms/100 initial U atoms (see sample 2-1);
$(conc)_{Ru}$ = 4.75 atoms/100 initial U atoms (see sample 2-1);
$(conc)_{Pd}$ = 2.01 atoms/100 initial U atoms (see sample 2-1);
$(conc)_{U}$ = 100 - 25 = 75.

The amount of Mo, Ru, and Pd added to the 90% UO_2/10% UC_2 mix was increased by a factor of 2.5 in order to assure ourselves that we would be able to detect them by dispersive x rays. No new phases were introduced at this level. Above factors of 2.5, another phase begins to appear.

In weight percent:

Mo =	$(5.94 \times 2.5) \times 95.94$	= 1,425 =	6.10%
Ru =	$(4.75 \times 2.5) \times 101.07$	= 1,207 =	5.17%
Pd =	$(2.01 \times 2.5) \times 106.91$	= 538 =	2.30%
UO_2 =	$(75.0) \times (270.04) \times 0.90$	= 18,227 =	78.07%
UC_2 =	$(75.0) \times (260.06) \times 0.10$	= 1,950 =	8.35%
		23,347	

Sample 2-7 (65% UO_2/35% UC_2 plus Mo-Ru-Pd)

[Assume 20% ^{235}U enrichment and 25% FIMA (13.75% ^{235}U; 11.25% ^{239}Pu)]

$(conc)_{Mo}$ = 5.94 atoms/100 initial U atoms (see sample 2-1);

$(conc)_{Ru}$ = 4.75 atoms/100 initial U atoms (see sample 2-1);

$(conc)_{Pd}$ = 2.01 atoms/100 initial U atoms (see sample 2-1);

$(conc)_{U}$ = 100 - 25 = 75.

The amount of Mo, Ru, and Pd added to the 65% UO_2/35% UC_2 mix was increased by a factor of 2.5 in order to assure ourselves that we would be able to detect them by dispersive x rays. No new phases were introduced. Above factors of 2.5, another phase begins to appear.

In weight percent:

Mo =	$(5.94 \times 2.5) \times 95.94$	= 1,425 =	6.15%
Ru =	$(4.75 \times 2.5) \times 101.07$	= 1,207 =	5.21%
Pd =	$(2.01 \times 2.5) \times 106.91$	= 538 =	2.32%
UO_2 =	$(75.0) \times (270.04) \times 0.65$	= 13,164 =	56.84%
UC_2 =	$(75.0) \times (260.06) \times 0.35$	= 6,827 =	29.48%
		23,161	

Sample 2-8 (UO_2 plus Ag)

[Assume 20% ^{235}U enrichment and 25% FIMA (13.75% ^{235}U; 11.25% ^{239}Pu)]

$(conc)_{Ag}$ = $(0.1375 \times 0.033) + (0.1125 \times 1.65)$ = 0.190 atoms/100 initial U atoms;

$(conc)_{U}$ = 100 - 25 = 75.

The amount of Ag added to the UO_2 was increased by a factor of 4 in order to detect it by dispersive x rays. No new phases were introduced.

In weight percent:

$$\begin{aligned} Ag &= (0.190 \times 4) \times (107.87) = 80 = 0.39\% \\ UO_2 &= (75.0) \times (270.04) = \underline{20{,}253} = 99.61\% \\ &\qquad 20{,}333 \end{aligned}$$

Sample 2-9 (UO_2 plus CdO-SrO)

[Assume 20% ^{235}U enrichment and 25% FIMA (13.75% ^{235}U; 11.25% ^{239}Pu)]

$(conc)_{Cd}$ = (0.1375) x (0.067) + (0.1125)(0.575) = 0.0739 atoms U/100 initial U atoms;

$(conc)_{Sr}$ = (0.1375) x (9.565) + (0.1125)(3.481) = 1.707 atoms U/100 initial U atoms;

$(conc)_U$ = 100 - 25 = 75.

The amount of Cd added to UO_2 was increased by a factor of 100 and the amount of Sr added was increased by a factor of 10 in order to assure ourselves that we would be able to detect them by dispersive x rays. No new phases were introduced.

In weight percent:

$$\begin{aligned} CdO &= (0.0739 \times 100) \times 128.41 = 900 = 3.93\% \\ SrO &= (1.707 \times 10) \times 103.63 = 1{,}770 = 7.72\% \\ UO_2 &= (75.0) \times 270.04 = \underline{20{,}253} = 88.35\% \\ &\qquad 22{,}923 \end{aligned}$$

Appendix C. *QUANTITATIVE DATA FOR LaC_2 AND NdC_2 INTERACTION WITH SiC*

Reference 10 of this report documents the thinning rate of SiC resulting from the interaction with LaC_2 and NdC_2. The raw data used to calculate the thinning rate are listed in Tables C.1 and C.2.

Table C.1. Raw data for LaC_2-SiC interaction in SiC-coated particles at 278°C/cm

Run No./ time (h)	Method used	Particle No.	Penetration of SiC (μm)	Temperature (K)
1/144	Metallography	4	18	2101
		5	16	2024
		6	18	2045
		8	15	1953
		9	10	1919
		10	11	1887
1/144	Radiography	7	14	2020
2/386	Metallography	4	6	1908
		9	5	1821
		10	5.5	1770
		13	3	1805
		14	4	1773
		15	3	1736
		17	2	1718
		19	2	1724
		20	3	1733
		21	6	1724
2/386	Radiography	1	10	1961
		2	7	1946
		3	7	1934
		5	10	1919
		7	7	1866
		8	7	1835
		12	4	1825
		16	6	1704
		18	7	1754
3/3428	Radiography	3	5	1669
		4	5	1684
		5	5	1672
		6	4	1661
		7	3	1645
		8	3	1637
		9	4	1616
		12	4	1608
		13	4	1650
		14	2	1575
		15	3	1580

Table C.1 (continued)

Run No./ time (h)	Method used	Particle No.	Penetration of SiC (μm)	Temperature (K)
4/90	Radiography	1	23	2174
		3	25	2174
		4	25	2123
		5	24	2114
		7	18	2045
		9	19	2024
		11	18	2004
		13	17	2020
		15	19	2058
		16	18	2058
		17	15	2020
		19	15	1996
		20	14	1976
		21	12	1949
		23	11	1908

Table C.2. Raw data for NdC_2-SiC interaction in SiC-coated particles at 278°C/cm

Run No./ time (h)	Method used	Particle No.	Penetration of SiC (μm)	Temperature (K)
1/144	Metallography	1	11	2179
		2	10	2155
		3	15	2062
		4	13	2101
		6	10	2033
		8	5	1949
		9	9	1984
		10	5	1996
		11	6	1927
		12	6	1908
1/144	Radiography	5	12	2092
		7	9	2016
4/187	Metallography	6	35	2128
		9	16	2141
		18	8	1880
		19	8	1869
		21	9	1873
4/90	Radiography	2	14	2193
		3	12	2174
		4	14	2174
		6	16	2128
		7	14	2119
		8	14	2105
		9	15	2141
		10	13	2114
		11	14	2146
		12	10	2092
		13	9	2062
		14	10	2020
		15	7	2000
		16	10	1965
		17	8	1912
		18	7	1880
		19	3	1869
		20	4	1887
		22	8	1887

Table C.2 (continued)

Run No./ time (h)	Method used	Particle No.	Penetration of SiC (μm)	Temperature (K)
6/500[a]	Radiography	1	9.7	2014
		5	18.4	1993
		6	14.1	1943
		8	12.9	1973
		10	20.3	1955
		11	18.3	1959
		12	12.9	1941
		14	13.2	1923
		15	13.9	1909
		16	13.7	1914
		18	13.3	1823
		22	10.0	1825
		23	13.1	1887
		24	14.2	1891
		26	6.7	1859
		30	19.0	1743
3/4265	Radiography	1	5	1682
		2	5	1641
		3	3	1567
		4	4	1576
		5	2	1590
		6	5	1571
		7	4	1474
		8	2	1488
		9	2	1464
		10	2	1451
		11	2	1488
		12	2	1529
		13	1	1511
		15	2	1469
		16	2	1423
		17	2	1404
		18	1	1372
		19	1	1381

[a]Linear fit of data obtained over 274 h. Calculations based on extension of lines to 500 h.